NASA CR-111785

HIGH POWER QUASI-STEADY MPD ACCELERATION

A. C. Malliaris, D. R. Libby and R. R. John

Prepared Under Contract No. NAS1-9298 by

Avco Corporation
Government Products Group
Systems Division
Wilmington, Massachusetts 01887

for

NATIONAL AERONAUTICS AND SPACE ADMINISTRATION
Langley Research Center
Langley Station
Hampton, Virginia 23365

NASA CR-111785

HIGH POWER QUASI-STEADY MPD ACCELERATION

A. C. Malliaris, D. R. Libby and R. R. John

May 1970

Final Technical Report
AVSD-0506-70-CR
Prepared Under Contract No. NASI-9298 by
AVCO CORPORATION
GOVERNMENT PRODUCTS GROUP
SYSTEMS DIVISION
Wilmington, Massachusetts 01887

for

NATIONAL AERONAUTICS AND SPACE ADMINISTRATION
Langley Research Center
Langley Station
Hampton, Virginia 23365

FOREWORD

This technical report was prepared by the Avco Corporation, Systems Division, Wilmington, Massachusetts, on Contract No. NAS1-9298 for the NASA/ Langley Research Center, Langley Station, Hampton, Virginia. The work reported was accomplished under the technical cognizance of Mr. J. Hoell, Mr. J. Burlock and Mr. R. Hess. The authors express appreciation to these individuals for their active interest in the present work and for their many helpful suggestions.

ABSTRACT

The first part of this report documents an investigation of ion-neutral coupling in plasma acceleration. The acceleration of a partially ionized gas by electromagnetic means is considered. This might be quite inefficient if the coupling between the ions and the neutrals for momentum transfer is weak. In the present work, the absence or presence of a sufficiently strong coupling is generally revealed by velocity disparities determined spectroscopically, for several species, both ionic and neutral. Velocities are determined by Doppler shift measurements of selected spectral lines. Results regarding two different situations are presented from experiments where two basically similar axisymmetric configurations operate under significantly different conditions. In the first case, a large disparity in ion-neutral velocities is observed. In the second case, the said disparity disappears and the common ion-neutral velocities are in good agreement with the center-of-mass velocity, as determined independently from measurements of motionally induced potentials in the flow. A satisfactory interpretation of the results is obtained when the calculated mean free path for momentum exchange is compared with a typical dimension of the electromagnetic acceleration region.

The second part of the report documents the preparation of a high power quasi-steady MPD for repetitive operation in the laboratory. Two topics receive particular consideration: (a) The generation of desirable mass flow pulses on a repetitive basis, and the diagnostics of such pulses by transient probing; and (b) The development of a repetitively operating shutter with exposure durations between a few hundred microseconds and a few milliseconds.

This shutter may operate in synchronization with the MPD activation sequence, and is useful in isolating the radiation from any desirable time phase of the MPD pulse.

TABLE OF CONTENTS

ILLUSTRATIONS

ILLUSTRATIONS

ILLUSTRATIONS (Concl'd)

TABLES

I. INVESTIGATION OF ION-NEUTRAL COUPLING IN PLASMA ACCELERATION

A. INTRODUCTION

Consider a propulsion device operating at any desirable values of thrust and mass flow rate. It is well known that in such a device the thrust power (and therefore the input power) is affected by the state of uniformity of the propellant velocity. Specifically, spatial and/or temporal profiles of the propellant velocity have been considered in the literature as sources of non-uniformity losses. Strictly speaking, the mentioned losses are not associated with any kind of power dissipation. Actually the losses reflect the fact that the power required for a given thrust, at a given flow rate, becomes increasingly larger, when the velocity non-uniformities become stronger.

Quantitative estimates of non-uniformity effects may be obtained from the following simple analysis. Consider two cases:

Case I. A mass flow rate $\dot{m}$ is uniformly accelerated to a velocity u, producing a thrust $F = \dot{m}u$, at the expense of a thrust power $P = F^2/2\dot{m}$.

Case II. In this case, the same total mass flow rate $\dot{m}$ has two components, $\dot{m}_1$ and $\dot{m}_2$. These components are respectively associated with velocities u_1 and u_2, thrust components $F_1 = \dot{m}_1 u_1$ and $F_2 = \dot{m}_2 u_2$, and thrust powers $P_1 = F_1^2/2\dot{m}_1$ and $P_2 = F_2^2/2\dot{m}_2$.

The mentioned cases have been constructed so that $\dot{m} = \dot{m}_1 + \dot{m}_2$. Moreover, assume that $F = F_1 + F_2$. In other words, assume that the total mass flow rate, the total thrust, and thus, the average specific impulse is the same in both cases. Under such conditions, it is straightforward to see that

$$P_1 + P_2 \geq P \tag{1}$$

where the equality sign holds when $u_1 = u_2$. Otherwise, when u_2/u_1 is different than unity, the total thrust power of Case II is always larger than the thrust power of Case I. The relative thrust power difference is found to be:

$$(P_1 + P_2 - P)/P = a_2(1 - a_2)\,[(u_2/u_1) - 1]^2 \cdot [(1 - a_2) + (a_2 u_2/u_1)]^{-2} \tag{2}$$

where a_2 is the mass flow fraction

$$a_2 = \dot{m}_2/\dot{m} = \dot{m}_2/(\dot{m}_1 + m_2) \tag{3}$$

associated with velocity u_2 in Case II. Equation (2) shows that the relative power difference is always a positive number, except it is zero, when $u_2 = u_1$. It is also interesting to note that for a given velocity disparity ratio, u_2/u_1, the relative power difference given by Eq. (2) has a maximum, when $a_2 = u_1/(u_1 + u_2)$. This maximum is given by:

$$[(P_1 + P_2 - P)/P]_{max} = [(u_2/u_1) - 1]^2 / (4u_2/u_1) \tag{4}$$

The aforementioned relations are conveniently illustrated in Figure 1. Here we plot the relative thrust power difference, designated as relative excess power, versus the mass flow ratio $\dot{m}_2/\dot{m}$, for three different values of the velocity disparity ratio. Note, in all cases of this figure, the total thrust, total mass flow rate, and the average specific impulse are, by definition, the same and are equal to the corresponding quantities of a flow with no velocity disparities. However, if a fraction, say 10 percent, of the flow has a velocity disparity ratio equal to 3, 10 or 30, then the excess thrust power correspondingly would be 25, 200 or 550 percent, of the thrust power required in the case of a uniform flow.

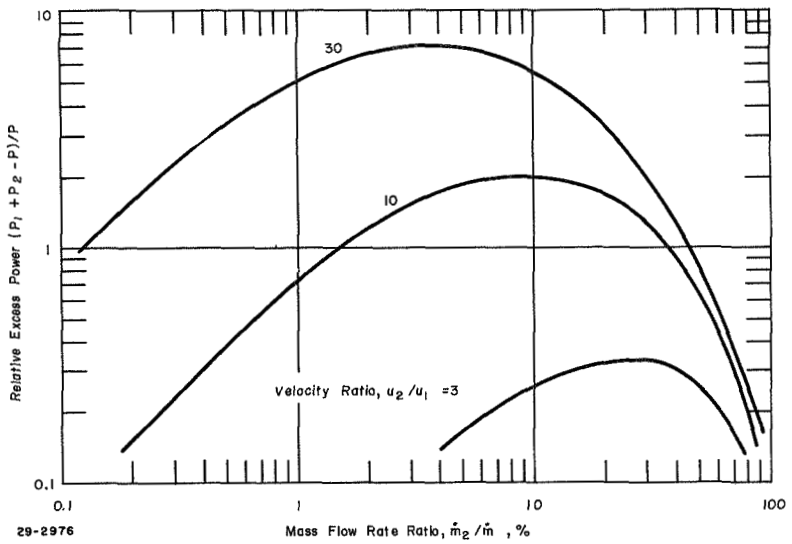

Figure 1 RELATIVE EXCESS POWER DUE TO NON-UNIFORMITIES VERSUS THE MASS FLOW FRACTION FOR THREE DIFFERENT RATIOS OF VELOCITY DISPARITIES

It is also realized that over and above the spatial and temporal non-uniformities mentioned, similar effects arising from velocity disparities in plasma flows where the propellant is a multi-component fluid must be considered. This is especially true in the acceleration of a partially ionized gas by electromagnetic means. Here the thrust power is originally invested in the ionic species of the flow. Consequently, large velocity disparities between the ions and the neutrals may arise, if the coupling for momentum transfer is weak.

The present work is concerned primarily with the investigation of ion-neutral velocity disparities in plasma flows of propulsion interest.

B. BACKGROUND

It is desirable to obtain a certain thrust from an MPD thrustor, ideally and most efficiently, by accelerating all the components of the propellant to a single axial velocity, with negligible radial gradients. In practice however,

the observed picture is distressingly different. This is especially so in the most usual, steady state MPD thrustor, operating at currents in the range of a few hundred amperes, external magnetic fields up to a few thousand gauss, and usually, with ammonia propellant at rates of the order of 10 mgm/sec.

Under such conditions, several investigators recently have observed and reported strong departures from a uniform axial flow velocity. These findings may be summarized as follows:

(a) The ionic species of the propellant have substantial rotational velocities (Refs. 1 and 2). This has been most readily demonstrated by the familiar slanting of ionic spectral lines, observed when the MPD flow is side-viewed (see Figure 2a). In this case, as would be expected from a rotating propellant, the part of the spectral lines originating from above the center line of the flow is Doppler shifted in one direction, while the opposite is true at the other end of the flow diameter. Generally, the mentioned rotational velocities increase with increasing MPD current and magnetic field. Comparison of Figure 2a with 2b, shows values comparable to the axial velocity of the propellant. Similarly, substantial rotational velocities have been measured and reported (Ref. 3) for ionized argon in an argon MPD flow.

(b) The presence of substantial rotational velocities of the ionic species, unjustified on gasdynamic grounds, leaves no doubt about the combined action of the electric and magnetic fields on the ionized part of the propellant. In this case, radial currents and axial B fields, and/or conversely, may combine to produce azimuthal acceleration. However, it is quite important to note (Refs. 1 and 2) that no evidence has been found

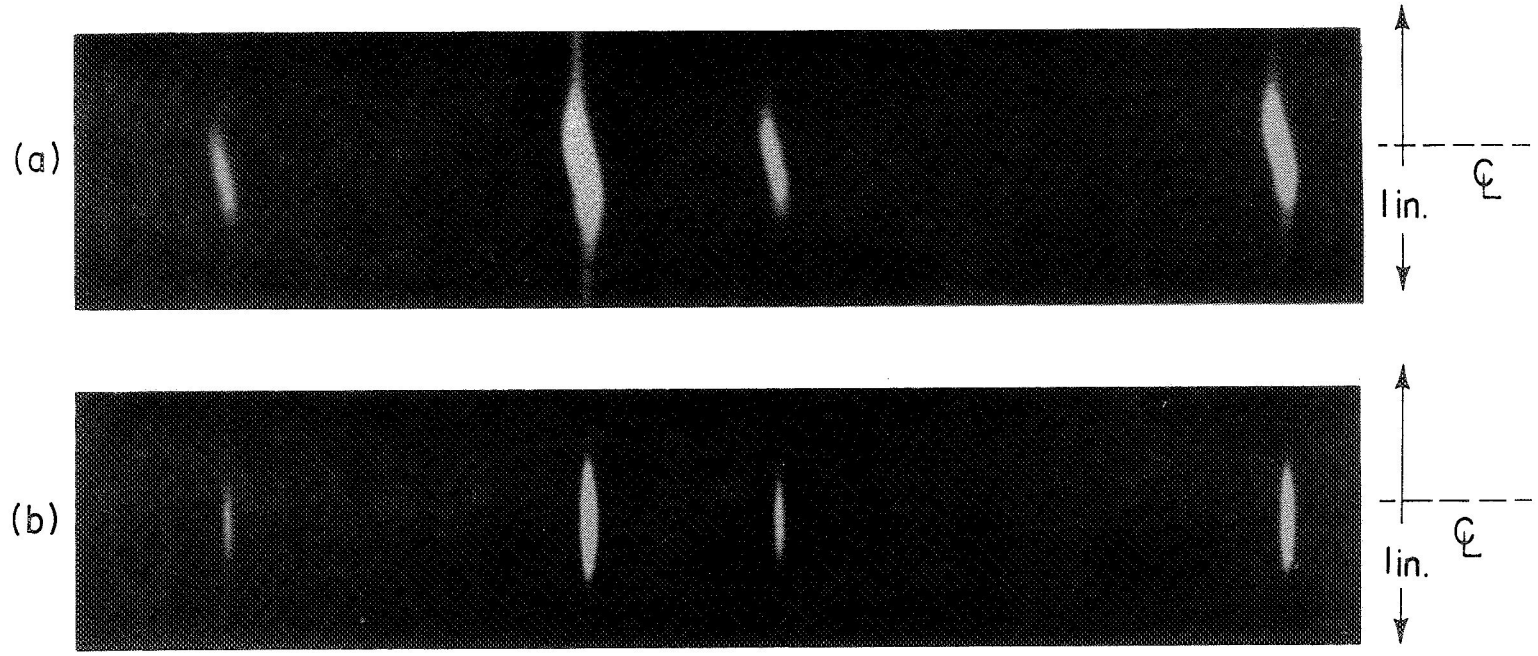

89-249

Figure 2 RADIALLY RESOLVED SPECTRAL LINES OF IONIZED NITROGEN, SHOWING A SUBSTANTIAL SLANTING DUE TO THE AZIMUTHAL MOTION OF THE PLASMA IN AN MPD FLOW OF NH_3 AT 20 mgm/sec. STRONGEST LINE AT 5680 Å. TOTAL SPAN ~27Å.
(Case (a) 800 Amperes -- 3000 Gauss)
(Case (b) 300 Amperes -- 400 Gauss)

indicating the neutral species in the same MPD flow have detectable rotational velocities. The familiar slanting effect of the ionic spectral lines is absent in the case of neutral lines. This is a definite indication of poor ion-neutral coupling, for momentum transfer.

(c) The situation of the observed axial velocities is more important, under the mentioned experimental conditions. Here again, very substantial disparities between ionic and neutral velocities have been reported (Refs. 1, 2, and 4). Generally, the neutral species have detectable velocities with values justified on gasdynamic grounds (thermal expansion), while the ions have velocities several times higher, justifiable only by virtue of electromagnetic acceleration. Other investigators (Ref. 5) have also observed relatively modest ion-neutral velocity disparities. However, the same investigators have reported (Ref. 6) a rather complicated dependence of velocity disparities on the environmental pressure of an MPD flow.

(d) Further evidence, regarding the weak coupling of the propellant species, was found (Ref. 1) in terms of the relatively strong dependence of the particle velocities (both ionic and neutral) on the particle mass. In these experiments, small amounts of various noble gases were added in the regular propellant. It was found that the particle velocities depend, not only on the ionic or neutral state of a particle, but also on its mass. Clearly, the heaviest particles were found to have the lowest velocities. Such a situation could not arise if the particles were strongly coupled for momentum transfer.

In conclusion, the findings indicate that the velocity field in typical, steady MPD flows is rather complicated and very non-uniform. Specifically, the

ionic species of the propellant appear to gain not only axial, but also rotational kinetic energy from electromagnetic forces. Conversely, the neutrals have much lower velocities, mostly of gasdynamic origin. Moreover, for all practical purposes, the neutrals are weakly coupled to the ions, and share little of the momentum electromagnetically gained by the ions.

C. EXPERIMENTAL ARRANGEMENTS

In addition to information discussed in the previous section, further experimental work is reported here, regarding the determination of ion-neutral velocity disparities in MPD flows. In these more recent experiments, two MPD configurations were employed as shown in Figures 3a and b.

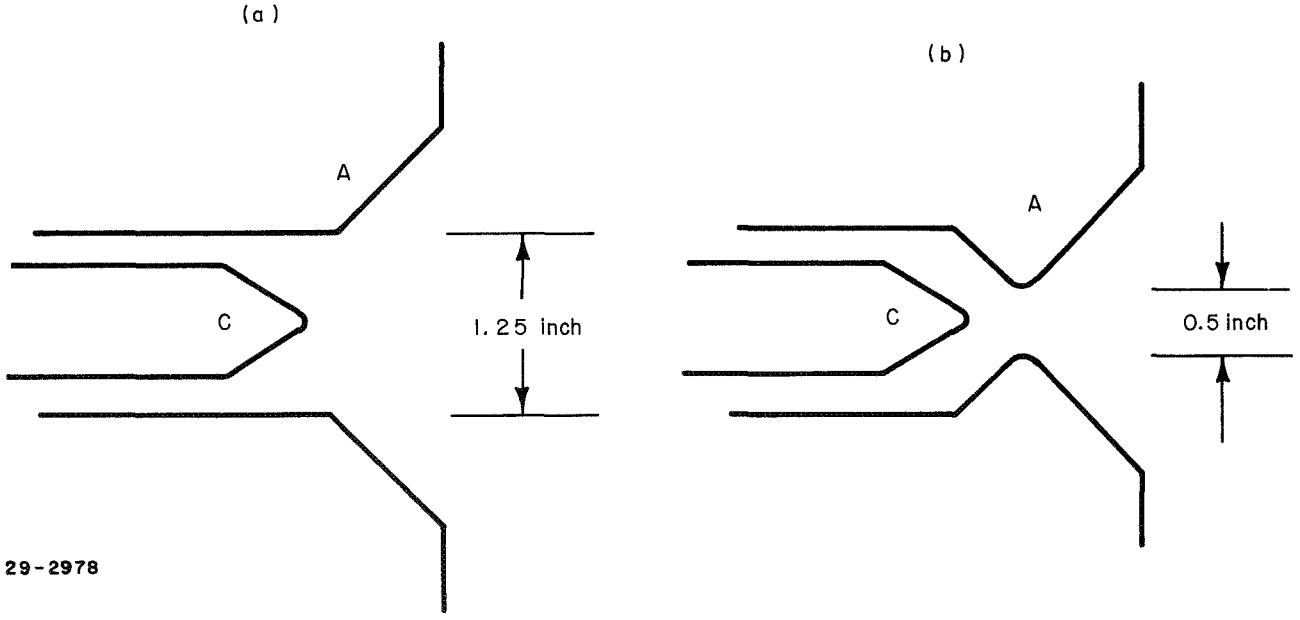

Figure 3 TWO MPD CONFIGURATIONS EMPLOYED IN THE EXPERIMENTS
(A : Anode, C : Cathode)

The corresponding ranges of experimental conditions are summarized in Table I. A comparison of the present arrangements and conditions with typical (Refs. 1 through 6) MPD conditions basically shows the mass flow rate has

been increased by one to two orders of magnitude, the current has been increased by a factor as large as 5, the externally applied B field has been made either very small or zero, and the input power has been increased by roughly an order of magnitude.

TABLE I

EXPERIMENTAL CONDITIONS REGARDING THE CONFIGURATIONS OF FIGURE 3

	Configuration (a)	Configuration (b)
Gas:	Ammonia and/or Nitrogen	Nitrogen
Flow Rate:	10 to 100 mgm/sec	100 to 500 mgm/sec
Chamber Pressure:	2 to 4 mm Hg	30 to 100 mm Hg
Environmental Pressure:	10 to 100 microns Hg	40 to 80 microns Hg
B field	< 300 gauss	zero
MPD Current	1000 to 2000 A	1000 to 2000 A
Power Input:	50 to 120 kW	40 to 100 kW
Additives, (in very small fractions):	Helium, Argon, Neon and Krypton	Helium, Argon, Neon and Krypton

These experimental conditions are by no means suggestive of more attractive MPD conditions for practical applications. The conditions are simply employed for the investigation of the problem of ion-neutral coupling in MPD flows. The following motivation is relevant. First, the drastic increase of the mass flow rate is intuitively clear. As will be explained later, the absence of strong ion-neutral coupling in typical MPD devices can be assigned to insufficient particle densities in the acceleration region. Obviously then, a large increase of the flow rate, without correspondingly large increases in flow cross-section and axial velocity, could help in strengthening the coupling in question. However, it is also understood that a drastic increase of the particle density does

not necessarily promote good ion-neutral coupling, unless accompanied by adequate ionization.

Thus, intuitively speaking, a stronger ion-neutral coupling when an increased mass flow rate is accompanied by an increase of the power input can be expected. The power increase, in the present experiments, was obtained mostly by an increase of the MPD current. This was not only necessary, but also very desirable. At high currents, the self-induced magnetic field ($\sim$ 1000 gauss at 2000 Amperes) may be as adequate as typical externally applied B fields. At the same time, the azimuthal self-field is more preferable, because, unlike an externally applied B field, it does not promote the familiar spoke formation and rotation (Ref. 7). The formation and rotation of spokes in MPD arcs is undesirable for several reasons. The most important reason is that a spoke may engage only a small fraction of the propellant in the electromagnetic interaction region, which concludes the motivation for conducting the present MPD experiments under the conditions of Table I.

Initially, experiments were performed with configuration (a) of Figure 3 and Table I. As will be seen in the detailed results of Section II, no evidence of strong ion-neutral coupling was found, even at flow rates as high as 100 mgm/sec. The mass flow rate could not be increased above this level, in configuration (a), without the onset of gross instabilities in the MPD accelerator. In fact, even at lower flow rates, a small external B field ($<$ 300 gauss) had to be applied to prevent gross instabilities. Configuration (b) of Figure 3 and Table I was then adopted as a desirable alternative for operating at higher flow rates. It was known from previous experiments (Ref. 8), that this configuration could operate without major problems at high flow rates, high currents, and zero

external B field. It is also important to note that, in configuration (b), advantage may be taken not only of higher flow rates, but also of higher values of the mass flux through the energy addition region. This is evident by inspecting the two geometries of Figure 3.

The velocities and velocity disparities under consideration were determined spectroscopically by measurements of the Doppler shifts of selected spectral lines, for several species both ionic and neutral. Also, as shown in Table I, several additives in small* fractions were used to study the dependence of velocities and velocity disparities on the particle mass.

The experimental arrangement for the Doppler shift measurements has been described in detail (Ref. 1). The essential aspects are summarized schematically in Figure 4.

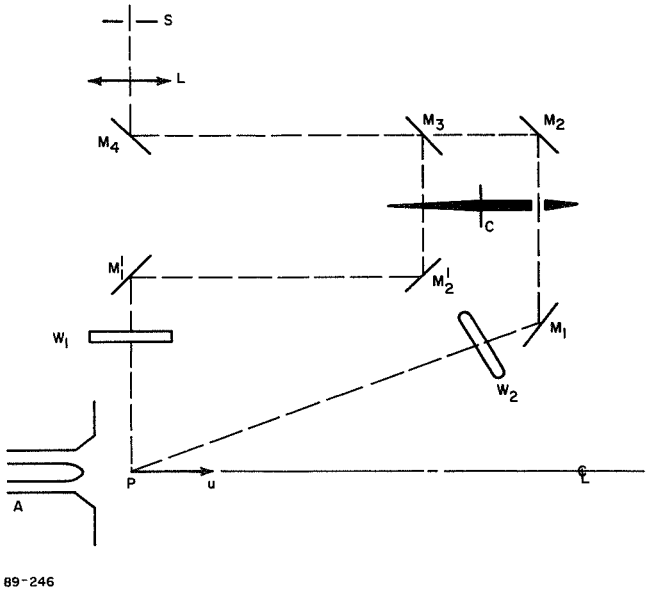

Figure 4 EXPERIMENTAL ARRANGEMENT FOR THE DETERMINATION OF DOPPLER SHIFTS DUE TO AXIAL MOTION
(A: Accelerator, W: Environmental Tank Windows, M: Mirrors, L: Lens, S: Spectrograph Entrance Slit, C: Chopper)

*Generally few percent or less of the main propellant flow, which was either ammonia or nitrogen.

The chopper substantially improves the sensitivity and reliability of this arrangement. It is used in such a way that either of the optical paths may pass while the other is blocked. This is done alternatively and repetitively, very many times, during any single scan of a spectral line. As a result of this, the radiation from both optical paths under comparison has one and the same wavelength scale, while individual scales can be conveniently maintained for the relative intensities.

Examples of Doppler shifts, measured photoelectrically and recorded on Polaroid pictures, are given in Figures 5a and b. The experimental arrangement is frequently tested against shifts of non-Doppler origin, by the use of a stationary source of radiation. The results of such a test are given in Figure 5c, where an expected zero shift is observed. Also, as a test, the side path of Figure 4, which provides the unshifted wavelength, has been replaced in several cases by a path originating from a stationary source, independent of the MPD flow. Such test measurements differ from ordinary measurements by less than $\pm$10 percent.

Strictly speaking, the Doppler shift measurements reported here are not spatially resolved. Most of the measurements refer to the core, (1/2 to 3/4 inch) of the MPD flow and have been obtained with line intensities and shifts integrated along lines of sight, passing through the centerline of the flow. However, the Doppler shift contributions, from the thicker and much slower gas layers surrounding the core, were effectively rejected. This was done by carefully selecting spectral lines which have strong intensities in the core, but much weaker intensities outside the core. Radial profile estimates of the axial velocities were obtained from auxiliary measurements, in which the Doppler shifts were observed along lines-of-sight off the center of the flow.

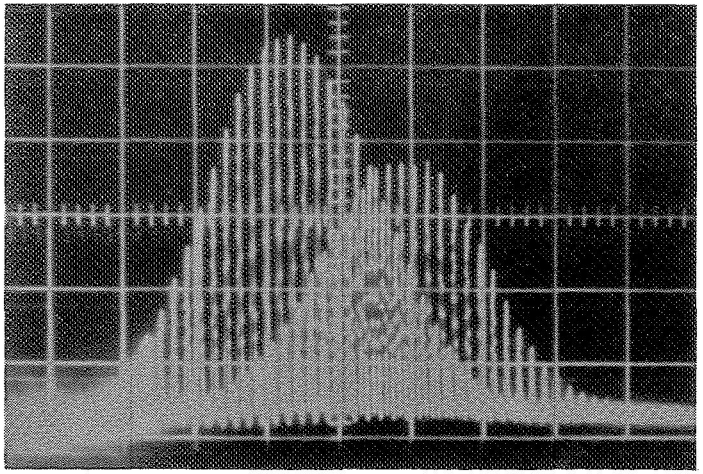

(a)

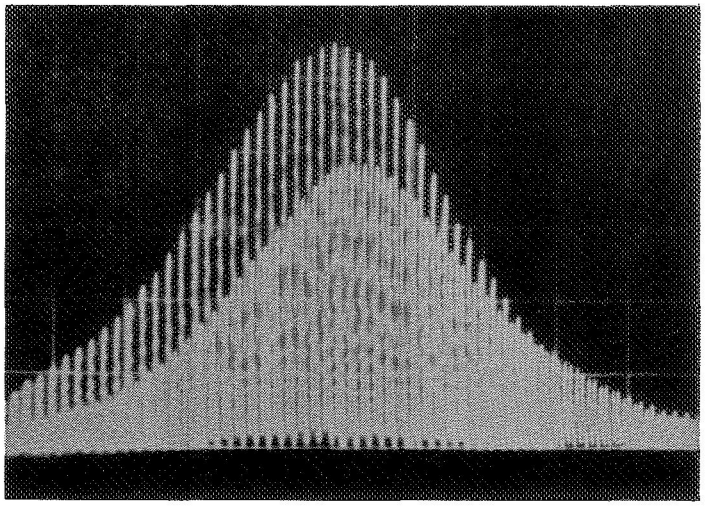

(b)

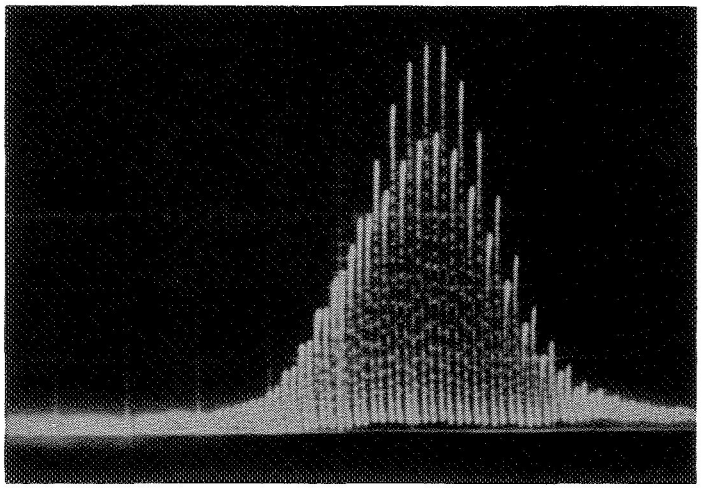

(c)

(a) Ionized nitrogen in an MPD flow

(b) Neutral hydrogen in an MPD flow, and

(c) Mercury from a stationary geissler tube. Total scan in each case: 1.25A

89-247

Figure 5 EXAMPLES OF SPECTRAL LINE SHIFTS

The most frequently used spectral lines, which qualified for the measurements reported here, are identified in Table II. It is noted that for one and the same particle, several wavelengths could be used. This was done frequently, as a test, in the determination of one and the same velocity, by using several different wavelengths. It is also noted that no spectral lines are available for the ions of hydrogen, helium and neon. In the case of hydrogen, naturally, no ionic lines exist, while the ionic spectral lines of helium and neon could not be excited, under the present conditions, because of their relatively high excitation potentials.

TABLE II

MOST FREQUENTLY USED SPECTRAL LINES

Species	Wavelength, $\mathring{A}$
Hydrogen Atom	6562 4861 4340
Helium Atom	6678 5875
Nitrogen Atom	7469 7443
Nitrogen Ion	5680 5005 3995
Neon Atom	6402 5852
Argon Atom	6965 7067
Argon Ion	4806
Krypton Ion	4659

D. EXPERIMENTAL RESULTS

Briefly and essentially, the results of this work show no evidence of strong ion-neutral coupling in the case of configuration (a), (Figure 3 and Table I). Moreover, ample evidence of strong coupling is found in the experiments with configuration (b), (Figure 3 and Table I).

1. Weak Ion-Neutral Coupling

Typical results regarding the weak coupling cases are illustrated in Figures 6 and 7 and in Table III. The velocities of Figure 6 refer to the core (1/2 to 3/4 inch) of the flow.

TABLE III

WEAK ION-NEUTRAL COUPLING
Dependence of Ion and Neutral Velocities, MPD Voltage and Plenum Pressure on the Accelerator Current, at $\dot{m}$ = 100 mgm/sec. Ammonia, and B < 300 gauss

I Amperes	V Volts	p_o mm Hg	Neutrals u^o 10^5 cm/sec	Ions u^+ 10^5 cm/sec
1,000	50	5	5.9	20
1,500	55	4	5.6	20
2,000	60	4	5.5	19.5

Ionic velocities are based mostly on nitrogen ions which occur naturally in an ammonia flow, while atomic hydrogen, also naturally occurring in the same flow, has provided the neutral velocities. Each point represents a straight average of many measurements, at least four or more, and the bars indicate the typical spread of these measurements. It is clearly seen that the ions are accelerated from relatively low velocities, in the vicinity of the

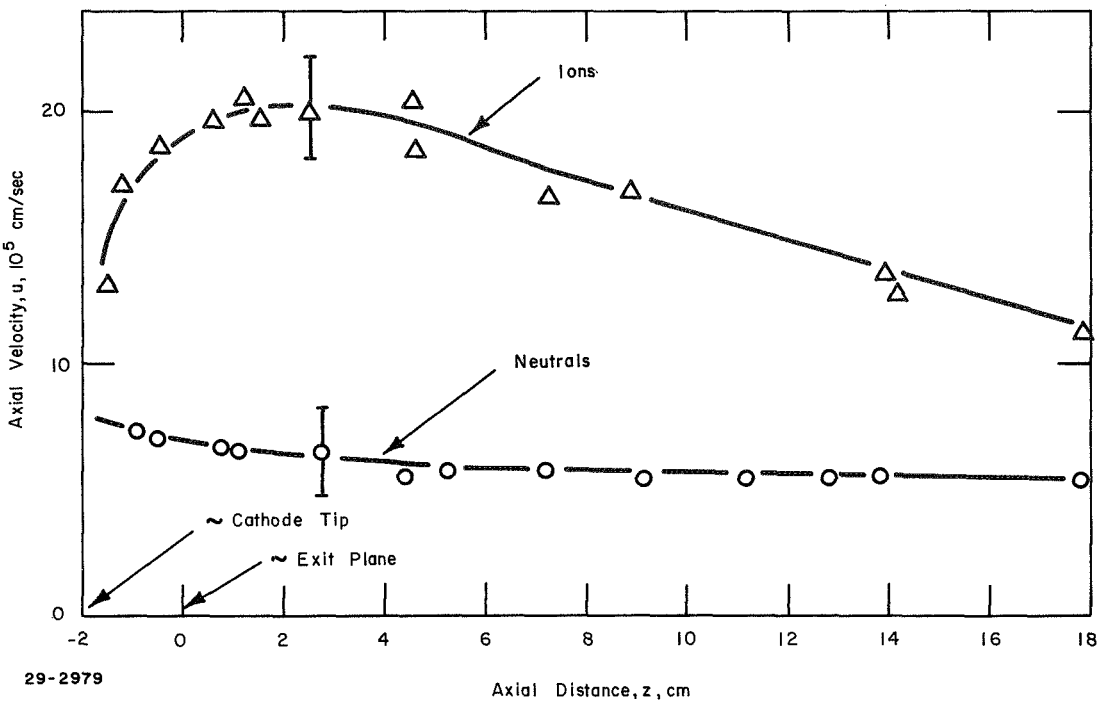

Figure 6 WEAK COUPLING
(Data Regarding Configuration of Figure 3a. Ammonia Flow at 100 mgm/sec, 1500 Amperes, with B ≤300 Gauss)

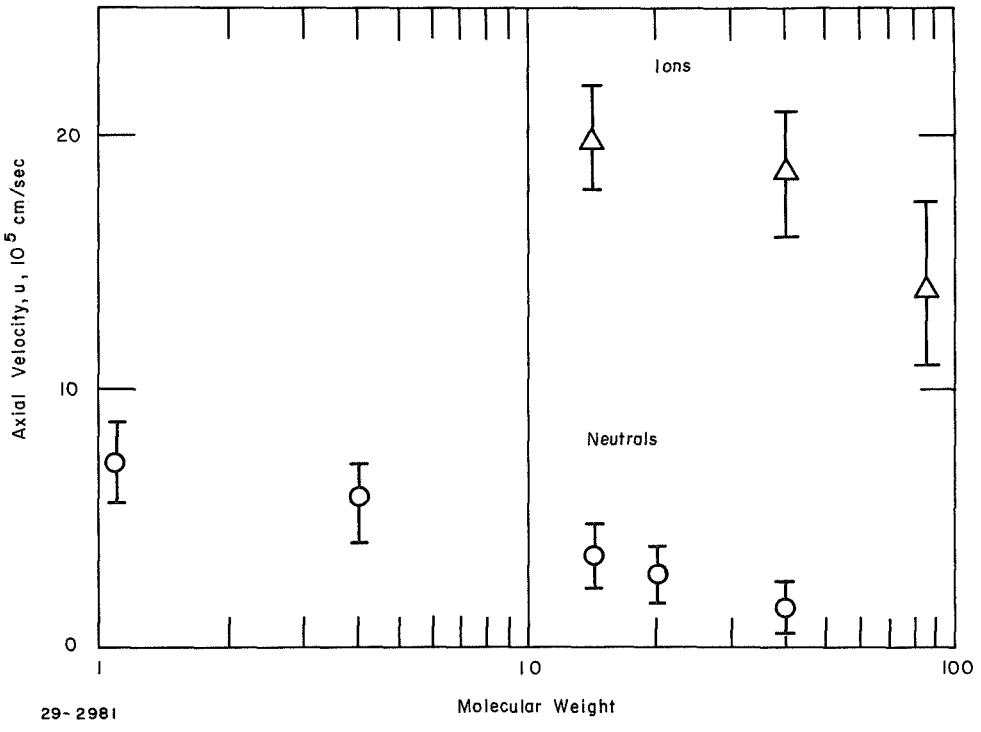

Figure 7 WEAK COUPLING
(Data Regarding Configuration of Figure 3a. Ammonia Flow at 100 mgm/sec, 1500 Amperes, with B ≤300 Gauss)

cathode,* to velocities just over 2 x 10^6 cm/sec. These ionic velocities decay rather slowly as the ions travel axial distances of many flow diameters downstream of the accelerator exit. At the same time the much slower neutrals show no evidence either of original acceleration or of momentum gain at the expense of ionic momentum, further downstream. Apparently, the slow decay of ionic velocities at large axial distances reflects the core decay of the MPD flow, by mixing. In this case, the ionic momentum loss is transferred to much larger amounts of gas. The neutrals might have small velocity gains which are hardly detectable. Regardless of these considerations, the very large disparities between ionic and neutral velocities clearly indicate the absence of good coupling.

As mentioned, the ionic velocities of Figure 6 refer to nitrogen ions, while hydrogen atoms have provided the neutral velocities. However, the velocity disparities between ions and neutrals, of the same particle mass, are more serious than those reflected in Figure 6. This may be seen in the data of Figure 7, where ionic and neutral velocities are given versus the particle mass. Hydrogen, helium, nitrogen, neon, argon and krypton species are found at molecular weights equal to 1, 4, 14, 20, 40 and 80, respectively. In these experiments, small additive fractions of noble gases have been used in the main, ammonia, propellant. The velocities reported here refer, as always, to the flow core and have been obtained at an axial distance, $\sim$ 3 cm, corresponding to the appearance of the board maximum in the ionic velocities, of Figure 6. The ion-neutral velocity disparities may be appreciated by reference to Figure 7, at a molecular weight equal to 14, nitrogen, and at

*Axial distances closer to the cathode could not be covered because of interference from the continuum radiation of the hot cathode.

40, argon. The data of Figure 7 also provide evidence showing a very substantial dependence of the particle velocity on the particle mass. This effect is especially strong for the neutrals and could not arise if a flow velocity common for all particles existed.

The data of Figures 6 and 7 do not change substantially for conditions other than those specified in the aforementioned figures, but within the ranges defined in Table I for configuration (a). Refer to Table III, which presents the dependence on the MPD current. Similarly, a variation of the mass flow from 10 to 100 mgm/sec does not alter the presented data significantly. Finally, as mentioned before, the external application of strong B fields introduces additional evidence of weak ion-neutral coupling, because in this case the ions acquire substantial rotational velocities, while the neutrals do not.

Before concluding this topic, it is worth noting that the neutral velocities of Table III are justifiable by gasdynamic considerations, while the ionic velocities are several times higher than average gasdynamic estimates. Such estimates may be obtained from the plenum pressures outlined in Table III, and from the ~ 8 cm^2 cross-section of the MPD throat shown in Figure 3a. For simplicity, a thrust coefficient equal to unity may be assumed. Then at 5 mm Hg plenum pressure and at 100 mgm/sec flow rate, we find an average gasdynamic velocity of 5.2×10^5 cm/sec, for the data of Table III.

2. Strong Ion-neutral Coupling

Typical results, illustrating the strong coupling cases are given in Figures 8 and 9 and in Table IV, which all refer to configuration (b) of Figure 3 and Table I. Again, all velocities refer to the flow core unless otherwise specified.

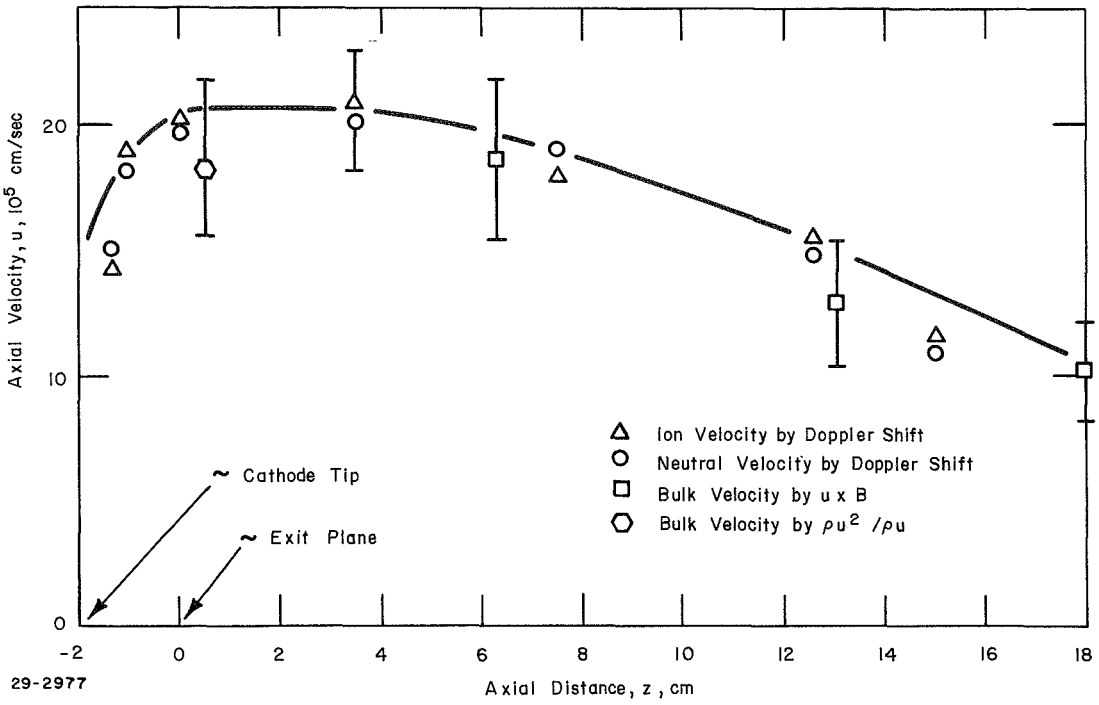

Figure 8 STRONG COUPLING
(Data Regarding Configuration of Figure 3b. Nitrogen Flow at 400 mgm/sec, 1500 Amperes B = 0)

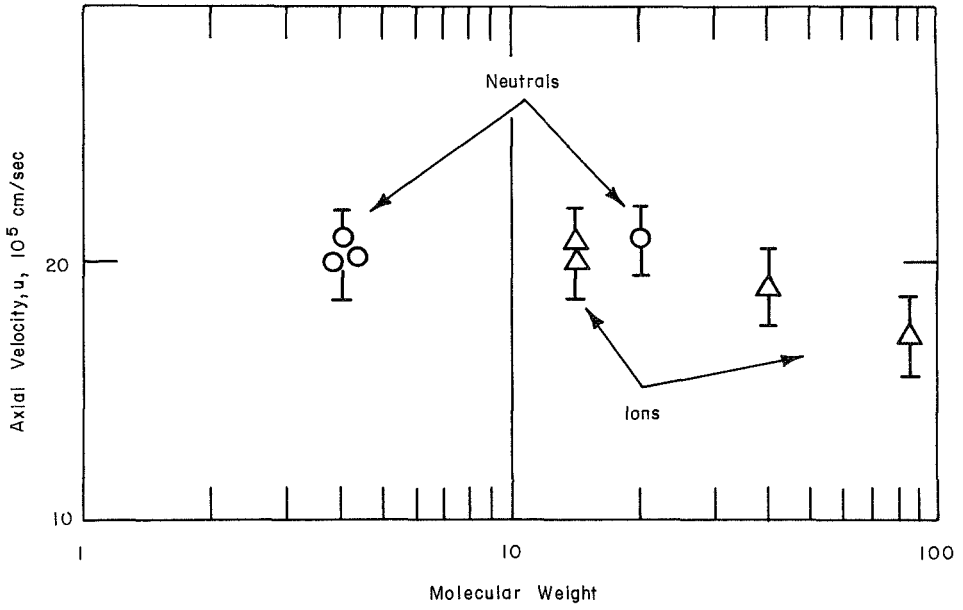

Figure 9 STRONG COUPLING
(Data Regarding Configuration of Figure 3b. Nitrogen Flow at 400 mgm/sec, 1500 Amperes and B = 0. All data at about 3 cm from the Accelerator Exit.)

TABLE IV

STRONG ION-NEUTRAL COUPLING
Dependence of Ion, Neutral, and Bulk Velocities on the Accelerator Current.
Also, MPD Voltage and Plenum Pressure, at $\dot{m}$ = 400 mgm/sec, Nitrogen and B = O

			Neutrals	Ions	Bulk
I Amperes	V Volts	p_o mm Hg	u^o 10^5 cm/sec	u^+ 10^5 cm/sec	$\langle u \rangle$ 10^5 cm/sec
1,000	40 ±5	60 ±5	16	17	15
1,500	43 ±5	70 ±5	21	20	19
2,000	47 ±5	85 ±5	23	23	24

The ion velocities of Figure 8 are determined by Doppler shift measurements and they are averages of many measurements made for nitrogen, argon and krypton ions. Similarly, the neutral velocities are averages obtained from many measurements with helium, nitrogen, neon, and argon neutrals. This averaging process is allowed here, both for ions and for neutrals, because the particle velocities are virtually independent of the particle mass, as may be seen in the data of Figure 9. Note that nitrogen is the main propellant and that all the noble gasses are small fraction additives. According to this evidence, all particles have a common velocity regardless of their ionic or neutral state and regardless of their mass. This common velocity increases rapidly in the acceleration region, close to the electrodes. It reaches values just over 2×10^6 cm/sec and it decays slowly at large axial distances, where copious mixing with the environmental gas may be taking place.

Two additional and independent velocity determinations have been superimposed on the ionic and neutral velocities of Figure 8. They are the bulk plasma velocity as determined by a $u \times B$ probe (Ref. 8), and the bulk

gasdynamic velocity, determined by combined momentum flux and mass flux probing (Refs. 8 and 9). In both cases, sufficient radial resolution was available for an average velocity determination in the flow core (1/2 to 3/4 inch). It is clear that all particle and bulk velocities plotted in Figure 8 are basically in agreement, as would be expected in a case of strong coupling between any two components of a fluid.

The discussed evidence of strong ion-neutral coupling is not detectably affected by a variation of the experimental conditions, as defined in Table I, for configuration (b). All velocities (neutral, ionic, and bulk) increase appreciably when the MPD current increases and/or when the flow rate decreases. However, a common velocity always remains in evidence, as may be seen in the data of Table IV.

E. ANALYTICAL CONSIDERATIONS

It is considered helpful to formulate a simple analysis for the interpretation and evaluation of the results regarding the ion-neutral coupling under the present experimental conditions as well as under more typical MPD conditions.

The present experimental data, Figures 6 and 8, clearly show that most of the acceleration (either for the ions or both for the ions and for the neutrals) occurs mainly between the cathode tip and the accelerator exit. This is not unexpected because the axial current density declines rapidly and becomes negligible outside the accelerator exit (Ref. 9). It must also be taken into account that the magnetic field is mostly self-magnetic. Thus, very little acceleration would be expected downstream of the accelerator exit. In other studies (Refs. 1, 2, and 6) under most typical MPD conditions (strong external B fields, much lower flow rates), substantial ionic acceleration takes place in

the region immediately downstream of the accelerator exit. This is also understood, because, under such conditions, substantial current densities are detected (Ref. 10) downstream of the accelerator exit, where substantial applied B fields also exist. In either case, the axially identified acceleration region also has been identified radially as a relatively small tube, confined in the core of the MPD flow. Such observations have been provided by current density probing (Ref. 10), and, in the present work, by auxiliary Doppler shift measurements.

The question of ion-neutral coupling is obviously meaningless when a totally ionized gas is considered. However, here we are interested in partially ionized flows, where ions are originally accelerated, and where any serious disparities between ion and neutral velocities are undesirable. Therefore, it is important to formulate a criterion, relevant to the strength of the coupling for momentum transfer from the ions to the neutrals.

Define, first, a radius R within which the plasma is confined and accelerated. This radius will be identified more precisely in the following analysis. However, it is already clear that R is not necessarily related to any hardware radius of the accelerator. This is especially so in the cases where the axial acceleration has been observed to take place, either downstream of the hardware exit of the accelerator, or at most within a flow core, with a small radius compared to a rapidly diverging hardware nozzle.

With the radius R so defined we suggest:

$$\lambda_o << R \tag{5}$$

as a criterion for strong ion-neutral coupling, where

$$\lambda_o = (1/n_+ Q_{ex}) \tag{6}$$

is the mean free path of a neutral between collisions with ions, for momentum exchange. In Eq. (6), we consider n_+ , the ion density, because only the ions are originally subject to confinement and acceleration forces. The momentum exchange crosssection, Q_{ex} , appearing in Eq. (6) has values (Ref. 11) generally between 5×10^{-16} and 5×10^{-15} cm^2, depending on the colliding particles and their relative velocity. The highest values are applicable in cases of resonant charge exchange, in collisions between ions and neutrals of the same atom.

The ion density is related to the total particle density in the plasma, n , by the relation:

$$n_+ = an \tag{7}$$

where a is the degree of ionization. A combination of Equation (5), (6) and (7) gives:

$$n R >> (1/aQ_{ex}) \tag{8}$$

When this criterion is satisfied, a strong coupling will be established between the ions and neutrals in the important region of the accelerator. Otherwise, the neutrals would leak out, while sharing very little of the momentum electromagnetically gained by the ions. An equally simple criterion could be applied for the axial acceleration of the neutrals. In this case, the radius R should be replaced by the axial dimension, L , of the acceleration region. However, from experimental studies we know that $L > R$, in most cases of interest. Thus, if criterion (8) is satisfied, then the condition for good ion-neutral coupling, in the axial direction, will also be satisfied.

For the evaluation of Equation (8), we clearly need the particle density and the confinement radius of the plasma in the acceleration region. The

following analysis appears to be relevant. First, it is noted that, no matter how strong the confining B field is, and how high the plasma conductivity is, there will always be a radial diffusion of the plasma across the B field. This also will be so regardless of the B field origin, external or self-induced. Let u_D be the diffusion velocity of the plasma. Clearly, if the plasma is accelerated over an axial length L , with an average velocity u_z , the confinement radius R will be augmented by:

$$\Delta R \simeq u_D \, (L/u_z) \tag{9}$$

In general we wish $\Delta R/R$ to be as small as possible, in the confinement and acceleration region of interest. Otherwise, the mass continuity will reduce the particle density, which is undesirable. Arbitrarily we set: $\Delta R/R \simeq 0.2$, which means an augmentation of the flow cross-section by about 50 percent, along the acceleration channel. Thus, relation (9) becomes:

$$u_D \simeq (u_z \, R/5L) \tag{10}$$

The radial diffusion velocity of the plasma may be related to other important parameters, as follows: The physical consequence of radial plasma diffusion against an orthogonal B field, (either axial and/or azimuthal), is the generation of an induced current density, j , given by:

$$j = \sigma \, u_D \, B \tag{11}$$

which is also orthogonal to both u_D and B . The plasma conductivity here, is represented by σ. In turn, the induced current density combines with the B field to provide a radial force, jB , which opposes and, in the steady state, balances the pressure gradient, ∇p, in the radial direction. This gradient may be approximated by p/R , where $p = nkT$ is the average plasma pressure, at an average plasma temperature T , inside R . When all relations, following Eq. (10), are combined, it is found that:

$$n/R^2 = (\sigma B^2/kT)(u_z/5L) \tag{12}$$

This relation alone is not adequate for the evaluation of Equation (8). Obviously, a second relation between n and R is needed. Intuitively, we feel that the mass continuity through the acceleration tube must be considered, because the mass flow rate has not appeared in the present analysis. For this, we write simply:

$$n\, m\, u_z\, \pi R^2 = \dot{m}$$

or

$$nR^2 = (\dot{m}/\pi\, m\, u_z) \tag{13}$$

where $\dot{m}$ is the mass flow rate* through the region of interest, and m is the average particle mass.

The particle density and the confinement radius in the acceleration region may be obtained from Equations (12) and (13) in terms of the quantities appearing on the right-hand sides. More important here is the product nR appearing in criterion (8). It is found that

$$nR = \left[(5\pi^3 L)^{-1} (\dot{m}/m)^3 (\sigma/kT)(B/u_z)^2\right]^{1/4} \tag{14}$$

A numerical evaluation of criterion (8) is now in order. We shall use Eq. (14) assigning values to the quantities of the right-hand side, as suggested by relevant experimental observations. Typical MPD conditions are considered first. It appears reasonable to take $u_z \simeq 10^6$ cm/sec as an average plasma velocity over an acceleration length $L \simeq 2$ inches. A magnetic field of 1000 gauss appears appropriate, and for a flow rate of 10 mgm/sec, ammonia or nitrogen,

*Not necessarily the metered flow rate.

for example we find: $(\dot{m}/m) \simeq 5 \times 10^{20}$. Finally with a typical temperature of 10^4 ^{o} K and for a conductivity of 10^3 mhos/m, we obtain: $nR \simeq 1.6 \times 10^{14}$ particles/cm^2. This results from a combination of 2×10^{14} particles/cm^3 with a confinement radius $R \simeq 0.8$ cm, as may be found by independently using Eqs. (12) and (13).

So far, there is nothing incredible in the values, estimated for n and R. However, throughout this analysis, the plasma has been treated as a single component fluid, and this may be physically acceptable, only if Equation (8) is satisfied. Reference to this relation shows that it is not satisfied, under the aforementioned MPD conditions. The right-hand side of Eq. (8) assumes the lowest value, of about 4×10^{14} cm^{-2}, when a degree of ionization is high* as 50 percent is combined with the upper limit of the exchange cross-section range, i.e., $Q_{ex} \simeq 5 \times 10^{-15}$ cm^2.

In summary then, typical MPD conditions require $nR \simeq 1.6 \times 10^{-14}$ cm^{-2} while the right-hand of criterion (8) could not possibly have a value lower than 4×10^{-14} cm^{-2}. Thus the criterion in question is not satisfied, and no strong ion-neutral coupling may be expected. Naturally, lower degrees of ionization imply an even weaker coupling. Otherwise, the sensitivity of criterion (8) to the particular experimental conditions may be evaluated when the right-hand side of Eq. (14) is inspected. Note that L, σ and T, which cannot be drastically altered in favor of stronger ion neutral coupling, have a rather wear influence (1/4 power), on nR. Similarly, B and u_z have a stronger influence, 1/2 power, but practical consideration would not allow much higher values for B, or much lower values for u_z, than assumed here.

---

*Much higher degrees of ionization would not be relevant in a problem of ion.neutral coupling.

Thus, it appears that $\dot{m}$ as a parameter could affect η_R, most significantly. This is so, not only because of the 3/4 power dependence in Eq. (14), but also because $\dot{m}$ may in principle be varied over a range much wider than that of any other parameter. A few comments are in order here, regarding the value of $\dot{m}$ which appears in Eq. (14), and is the actual flow rate through the acceleration region. As noted in connection with Eq. (13), $\dot{m}$ is not necessarily the metered value of the mass flow rate. This happens because the actual mass flow rate through the acceleration region may be seriously affected by two opposing influences. One is that a substantial fraction of the metered flow rate may altogether bypass the acceleration region, and the other is an environmental influence, namely, entrainment of gas from the environmental tank. In the concluding remarks, the aforementioned considerations are applied in the evaluation of three situations:

(a) The evidence of weak coupling (Refs. 1, 2 and 4) for typical MPD conditions, associated with previous work (Refs. 1 through 6).

(b) The evidence of weak coupling, associated with the data and conditions of Figure 6.

(c) The evidence of strong coupling associated with the data and conditions of Figure 8.

F. CONCLUDING REMARKS AND INTERPRETATION OF THE RESULTS

(a) Experimental work here (and in References 1, 2 and 4) shows no evidence of strong ion-neutral coupling in the case of typical MPD conditions, as defined in the discussion following Eq. (14). It is quite possible that, in these situations, a very substantial fraction of the metered flow rate bypasses the acceleration region. If this is a fact, then it is important to ask whether a strong coupling would be expected if all the

metered flow rate were passing through the acceleration region? The answer to this question appears to be negative, as shown by the discussion which follows Eq. (14). Regardless of this negative answer, one more outstanding question exists, namely, what determines and influences the fraction of the metered flow rate which is engaged in the acceleration region?

(b) The presence of weak coupling, under the conditions of Figure 6, is experimentally obvious. The question is whether this is analytically expected. The answer here is that the coupling is analytically expected to be weak, or at best marginal. This may be seen by repeating the procedure following Eq. (14). In the present case, the flow rate is 100 instead of 10 mgm/sec, ammonia, and the external B field is replaced by a comparable self-induced B field. Otherwise, the same general conditions are applicable. When Eq. (14) is used, it is found that $nR \simeq 9 \times 10^{14}$ cm^{-2}, which must be compared with 4×10^{14} cm^{-2} on the right hand side of Equation (8). Thus, the situation appears to be at best marginal, even when the full value of the metered flow rate is used in Eq. (14).

(c) Finally, the strong coupling of Figure 8 is both experimentally obvious and easier to justify analytically. Here, not only the flow rate is four times higher than in the last case, but also, the configuration is less favorable to the propellant bypassing the acceleration region. In this case, an application of Eq. (14) yields $nR \simeq 26 \times 10^{14}$ cm^{-2}, which must be compared with 4×10^{14} cm^{-2} on the right-hand side of criterion (8).

A few more comments are still necessary regarding the environmental interference known as entrainment. Regarding cases (b), and (c) above, it has been determined experimentally (Ref. 12) that, under the specified experimental conditions, entrainment is fractionally small. Quantitative experiments (Ref. 12),

with tracer gases in the environmental tank and sample taking from several flow stations, have shown that the fractional amount of the environmental gas in the MPD flow, varies between a few and ten percent, depending on axial and radial station.

Entrainment data, on a quantitative basis, are not available for case (a). However, qualitative evidence shows that substantial entrainment could be taking place. Fractionally, it could be well above ten percent, especially since the propellant flow rates are lower in this case. Nevertheless, it is important to note that copious entrainment could falsify the experimental evidence, only when such evidence indicates good coupling. If, as the case is here, the experimental evidence indicates poor coupling, in spite of the fact that environmental gas might enter copiously into the acceleration region, then the coupling could not become any stronger in the absence of entrainment.

II. HIGH POWER QUASI-STEADY MPD ACCELERATION

A. GENERAL INFORMATION

The ultimate objective of the program under consideration is the overall system evaluation of quasi-steady MPD accelerators, operating with power pulses of the order of 10 megawatts and durations of the order of 1 millisecond, at repetition rates of the order of 1 pulse per second. A substantial amount of information regarding quasi-steady plasma acceleration, on a single pulse basis, is already available (Ref. 13). This information is considered as the starting point. Thus, the typical thruster configuration of Reference 13 is adapted for our purposes and is shown in Figure 10. The accelerator plenum is fed with argon, or any other gas, through several holes drilled on the insulator back-plate. A short drum behind the back-plate is fed directly by the pulsed valve.

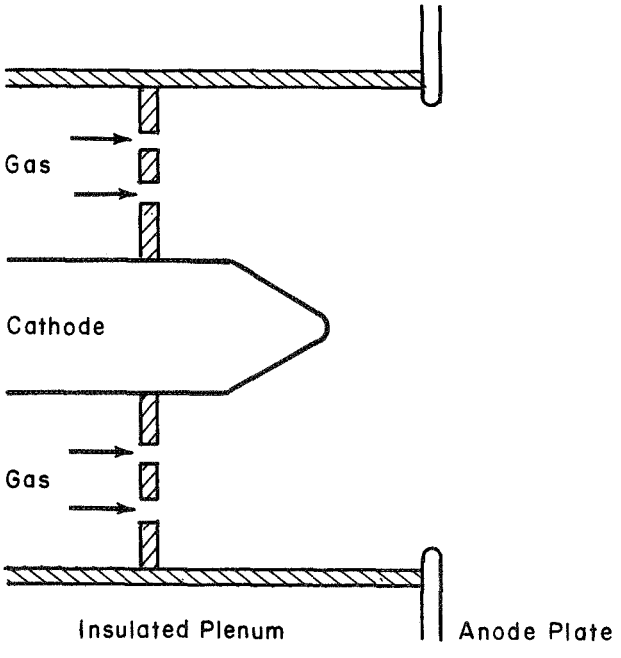

Figure 10 SCHEMATIC OF THE HIGH POWER ACCELERATOR
(Cathode: 3/4 inch Rod, Tungsten Tipped; Anode: Copper Plate, 2.5 inch Orifice; Cylindrical Insulated Plenum: 3 inch Diameter, 1.5 inch Deep)

Furthermore, for orientation purposes, Figures 11 and 12 present relevant information, also extracted from Reference 13. A virtually constant MPD impedance in the near vicinity of 10 milliohms is evident from the data of Figure 11. The dependence of this impedance on either the MPD current or on the mass flow rate is apparently very weak.

Figure 12 presents the current required for operation at a given power level. Again a very weak dependence on the mass flow rate is noted. Moreover, it is evident that MPD operation at pulse powers of the order of 10 megawatts will require currents well above 10 kiloamperes, regardless of the flow rate.

The three different values of the mass flow rate, indicated in Figures 11 and 12 are simply parameters. The choice of an appropriate value of the flow rate, for MPD operation at a certain power or current level, has been a matter of serious controversy for a long time. In our case, for reference purposes, we may estimate the required values of the flow rate on the basis of the expected thrust and of the desired specific impulse. The familiar expression relating the thrust to the square of the MPD current, $F = bI^2$, is applied for a rough estimate of the expected thrust. If (r_A/r_c), the ratio of anode to cathode current radii, is assigned a reasonable value, say 3, then the expected thrust varies from 2×10^3 to 4×10^4 gm of thrust, for MPD currents between 10 and 50 kiloamperes. Furthermore, if values of the specific impulse in the vicinity of a few thousand seconds are specified, it is seen that the appropriate mass flow rates should vary in the range of 1 to 20 gm/sec, during each pulse.

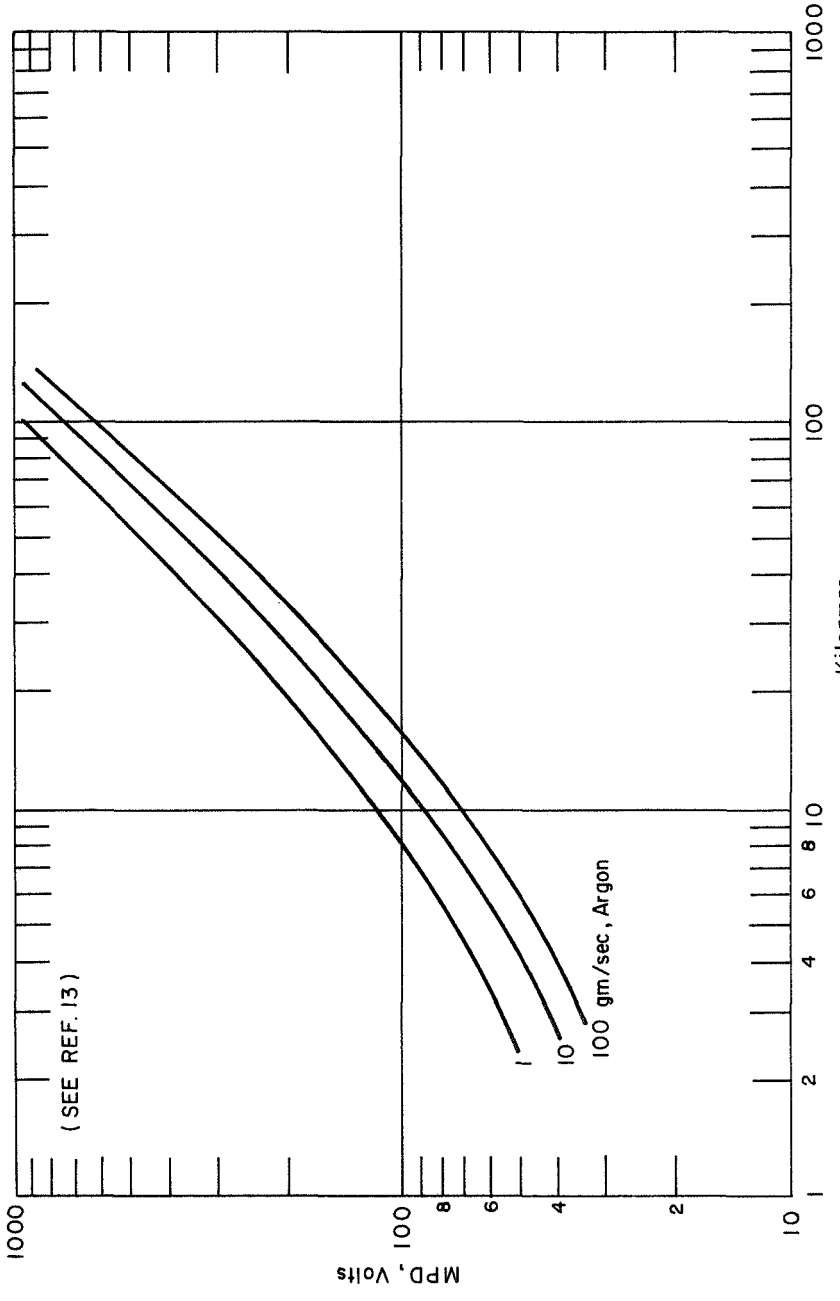

Figure 11 PULSED MPD VOLTAGE VERSUS CURRENT

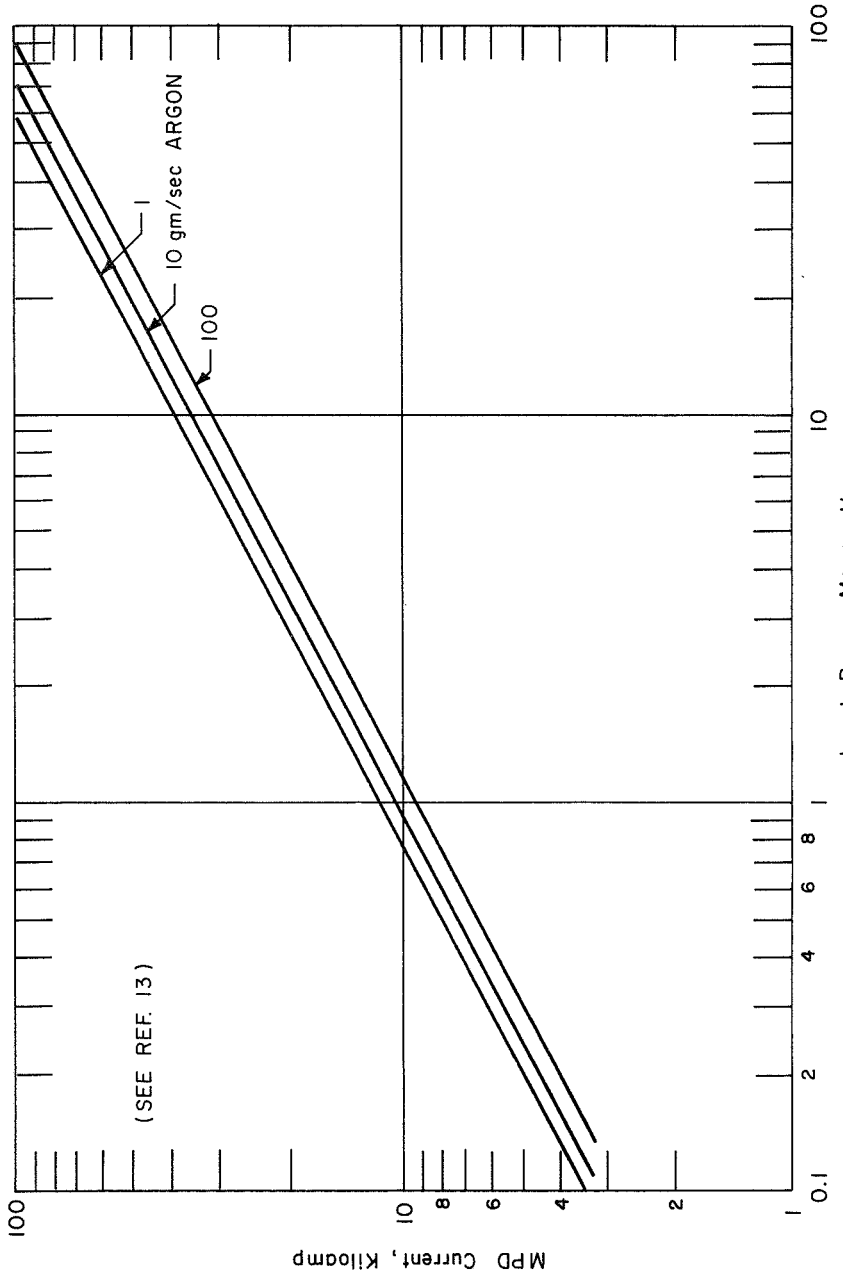

Figure 12 PULSED MPD CURRENT VERSUS PULSE POWER

With this general information in mind, we have proceeded to identify a pulsed valve assembly which could provide the mentioned flow rates at a repetitive rate of the order of 1 per second.

B. PULSED QUASI-STEADY MASS FLOW RATE

1. Pulsed Valve

No provision exists in the present program for the development of a pulsed valve. Accordingly, commercially available valves were examined and evaluated for possible application to our problem. The criteria of this evaluation were generally those just described. One family of valves, by no means unique, satisfying most of our general requirements is commercially available and manufactured by Skinner Electric Valve Division, Skinner Precision Industries Inc., New Britain, Connecticut.

A valve model, used quite extensively in our work, is identified as: Skinner Miniature Shut-Off, Two-Way Solenoid Valve, Normally Closed, Model No. C2LB1062. It is rated to operate continuously at 8 watts, 8 vac, 60 cps, and has a 5/32-inch orifice. Although rated at 60 SPI pressure, the valve has operated up to 150 PSI without obvious problems.

The most important modification in the operation of the aforementioned valve is the application of square voltage pulse with a few millisecond duration, and an amplitude much higher (up to 100 volts) than the steady state voltage recommended by the manufacturer. Such operation is easily tolerated by the valve solenoid at rep rates of 1 pps, while the onset of the $\dot{m}$ pulse in the accelerator region is very substantially sharpened.

The pulsed valve is activated by a simple power flip-flop circuit, sketched in Figure 13, with durations ranging from a few to 10 milliseconds. Generally speaking, the activation pulses have rise and fall times of the order of 100 microseconds, so they present no problem for the intended generation of millisecond $\dot{m}$ pulses.

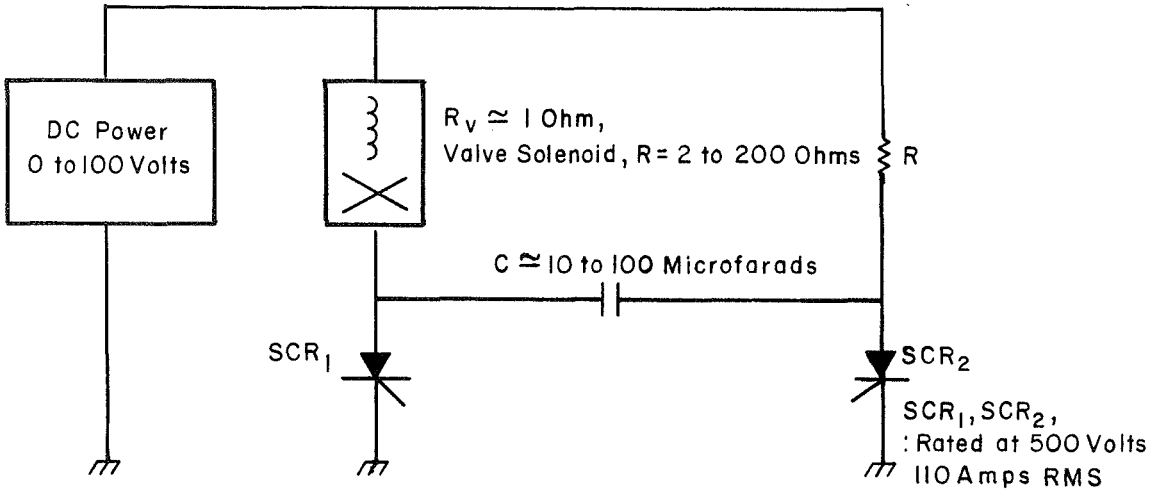

Figure 13 CIRCUITRY FOR PULSED VALVE ACTIVATION

2. Transient Pressure Gauge

The diagnostics of the $\dot{m}$ pulses were carried out with the help of a pressure gauge suggested by NASA/Langley. This is the Millitorr Ionization Gauge manufactured by Varian Associates and operated under the conditions recommended by the manufacturer. A calibration of this gauge is presented as Figure 14.

In our experiments, the ambient pressure is in the range 10 to 30 microns Hg, depending on the average mass flow rate. However, the

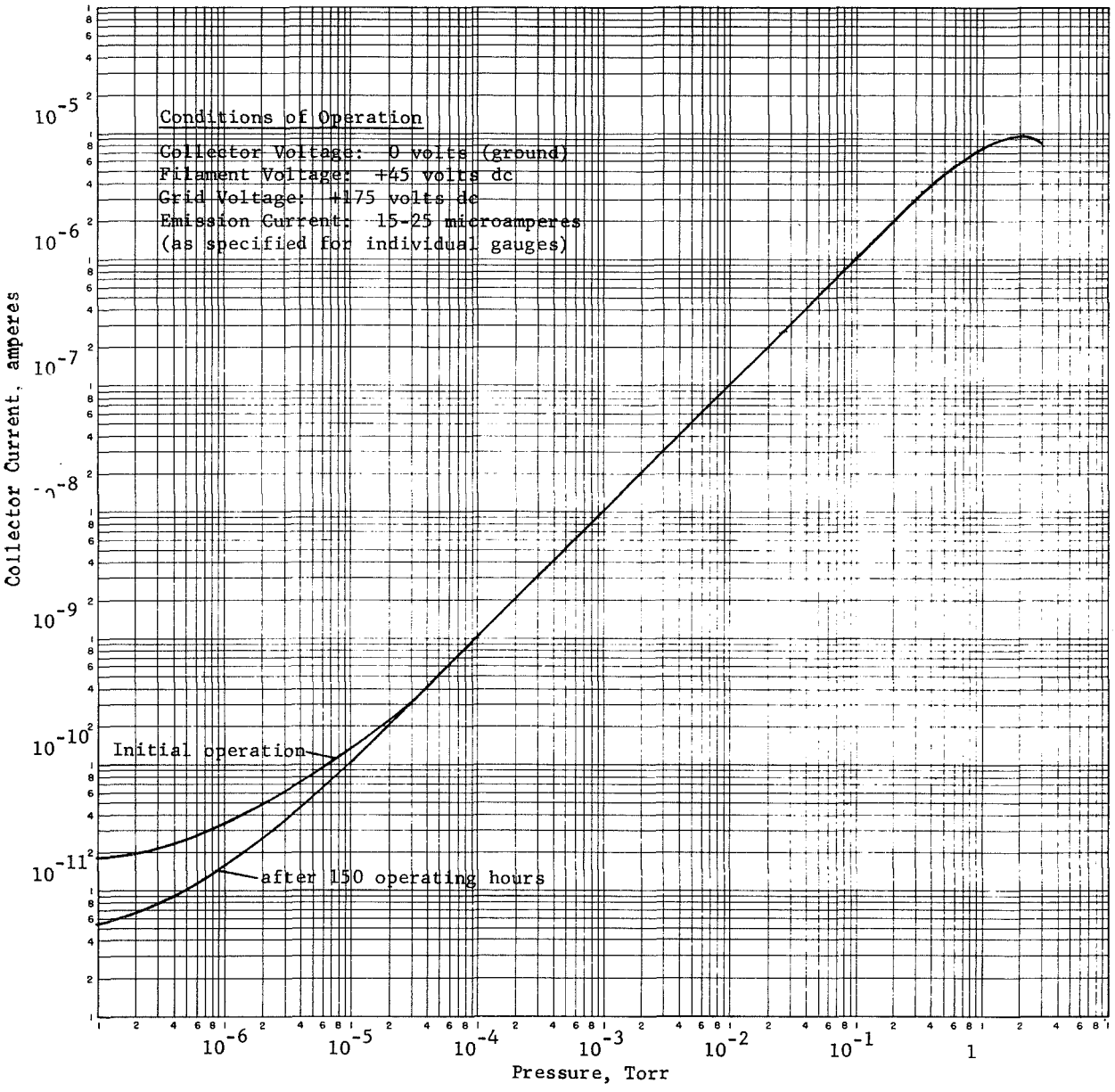

Figure 14 MilliTorr IONIZATION GAUGE CALIBRATION CURVE

pulse pressures could vary from the ambient pressure up to several millimeters Hg, depending on the values of $\dot{m}$ and on the probed station. Conversely, it must be noted that the transient pressure gauge has a linear response only up to 500 microns Hg. For our geometry and probing, see Figure 15, the pressure, even in the chamber, does not exceed this limit for mass flows as high as 10 gm/sec. Thus, the $\dot{m}$ pulse profiles, as diagnosed by the gauge, are not saturated for $\dot{m}$ values up to 10 gm/sec even in the accelerator chamber. Naturally, as the probing moves downstream, saturation is observed at progressively higher values of $\dot{m}$.

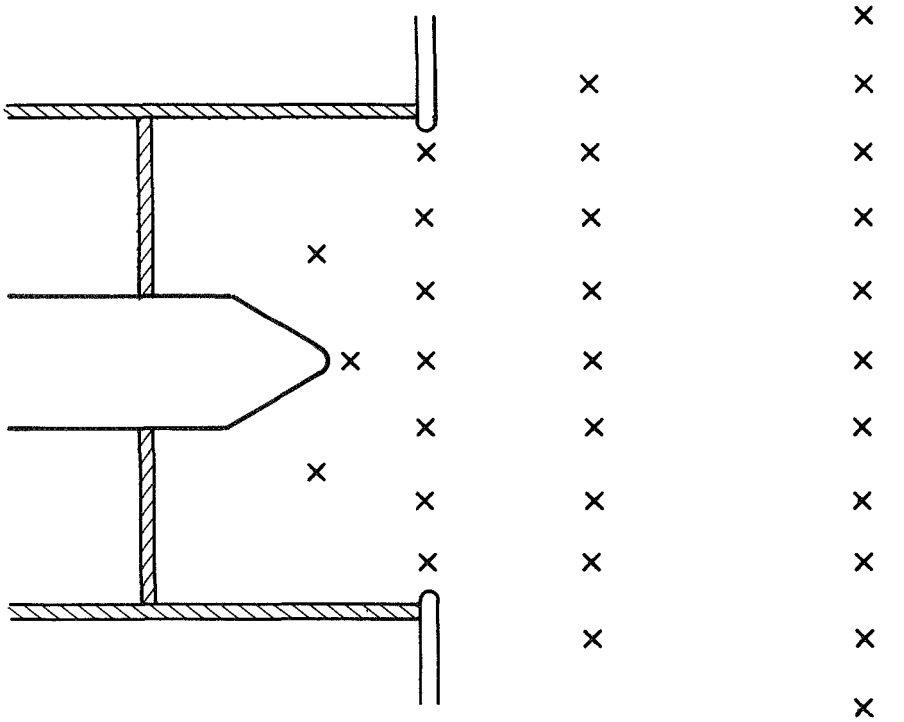

Figure 15 GENERAL GEOMETRY AND MATRIX OF POINTS PROBED BY TRANSIENT PRESSURE GAUGE

3. Additional Diagnostic Techniques

Over and above the use of the transient pressure gauge, one must use additional techniques for the diagnostics of the $\dot{m}$ pulses and for the calibration of the pulsed valve. A very useful quantity, for example, is the total mass expelled by the pulsed valve in a single pulse, namely the integral of $\dot{m}dt$. This quantity is easily measured when one or several

mass flow pulses are fed into a relatively small tank, of known volume, and the pressure rise is measured. This has been done, as a function of the activation time of a valve, in Figure 16, a straight line with a well defined shape is superimposed on a very substantial amount of expelled mass. This behavior indicates that the valve remains open (either in transients and/or in steady state) for durations substantially longer than the externally imposed activation times. However, it is also evident that a steady $\dot{m}$ is established for activation times above 2 milliseconds, because the slope of the plot in Figure 16 remains constant. In fact, this slope is a measure of the pulsed $\dot{m}$. The same slope is also linearly dependent on the reservoir pressure which, as expected, controls the magnitude of the pulsed $\dot{m}$. Relevant data are plotted in Figure 17, where, for comparison, flow rates determined by flow-meters, in steady tests of the same valve are presented.

As seen in Figure 17, the aforementioned valve covers $\dot{m}$ magnitudes between 3 and 25 gm/sec for argon reservoir pressures between 20 and 150 psia. Lower flow rates may be covered more conveniently with a smaller orifice valve. Similarly for $\dot{m}$ magnitudes above 20 gm/sec, a larger orifice is appropriate. Relevant data are presented in Figure 18.

Finally, it is worth noting that the valve(s) under consideration, pass a simple reproducibility test as shown in Figure 19, where the expelled mass per pulse is plotted for 10 consecutive pulses, both at the starting and ending phase of a several minute long operation, at 1 pps.

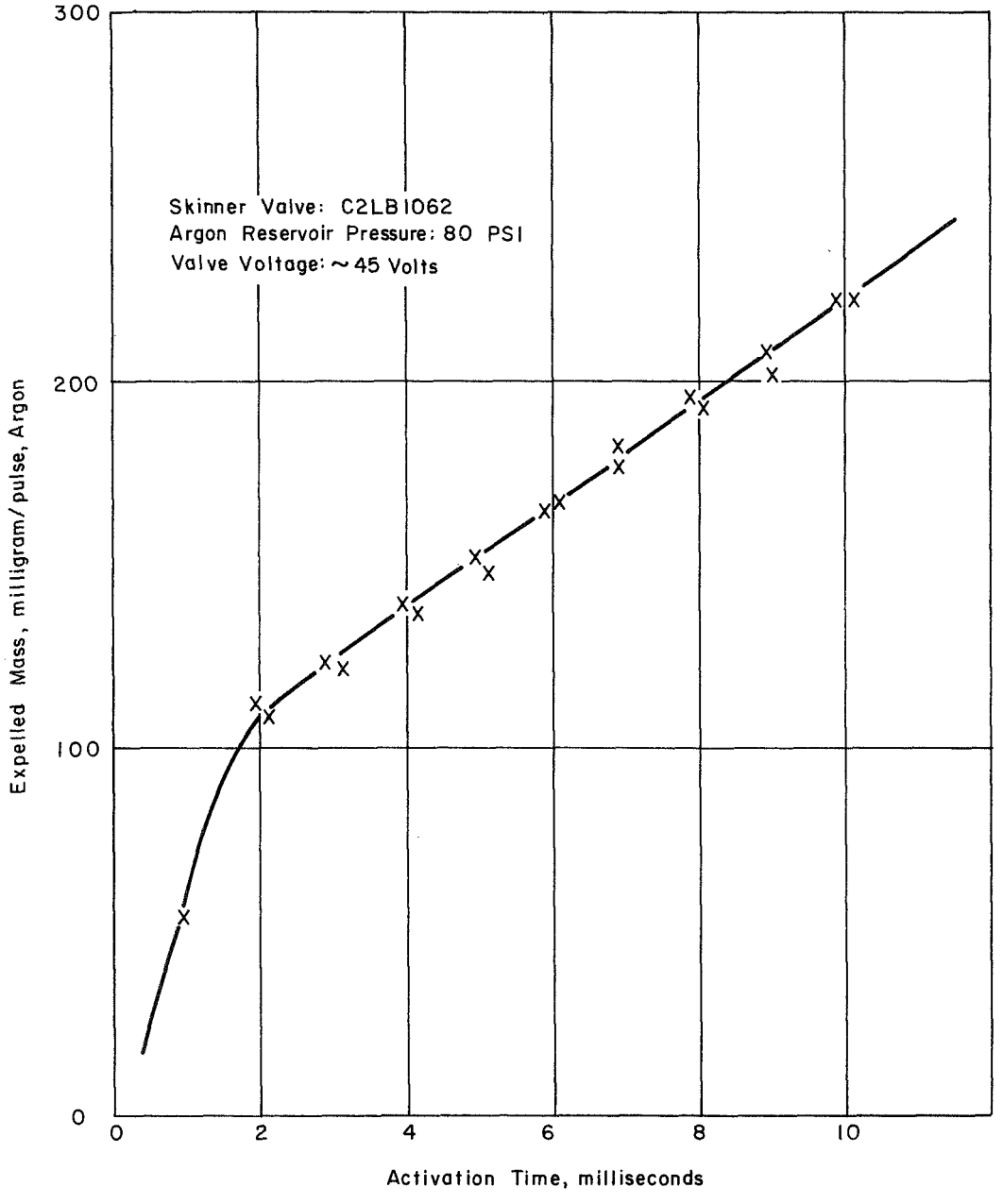

Figure 16 EXPELLED MASS VERSUS VALVE ACTIVATION TIME

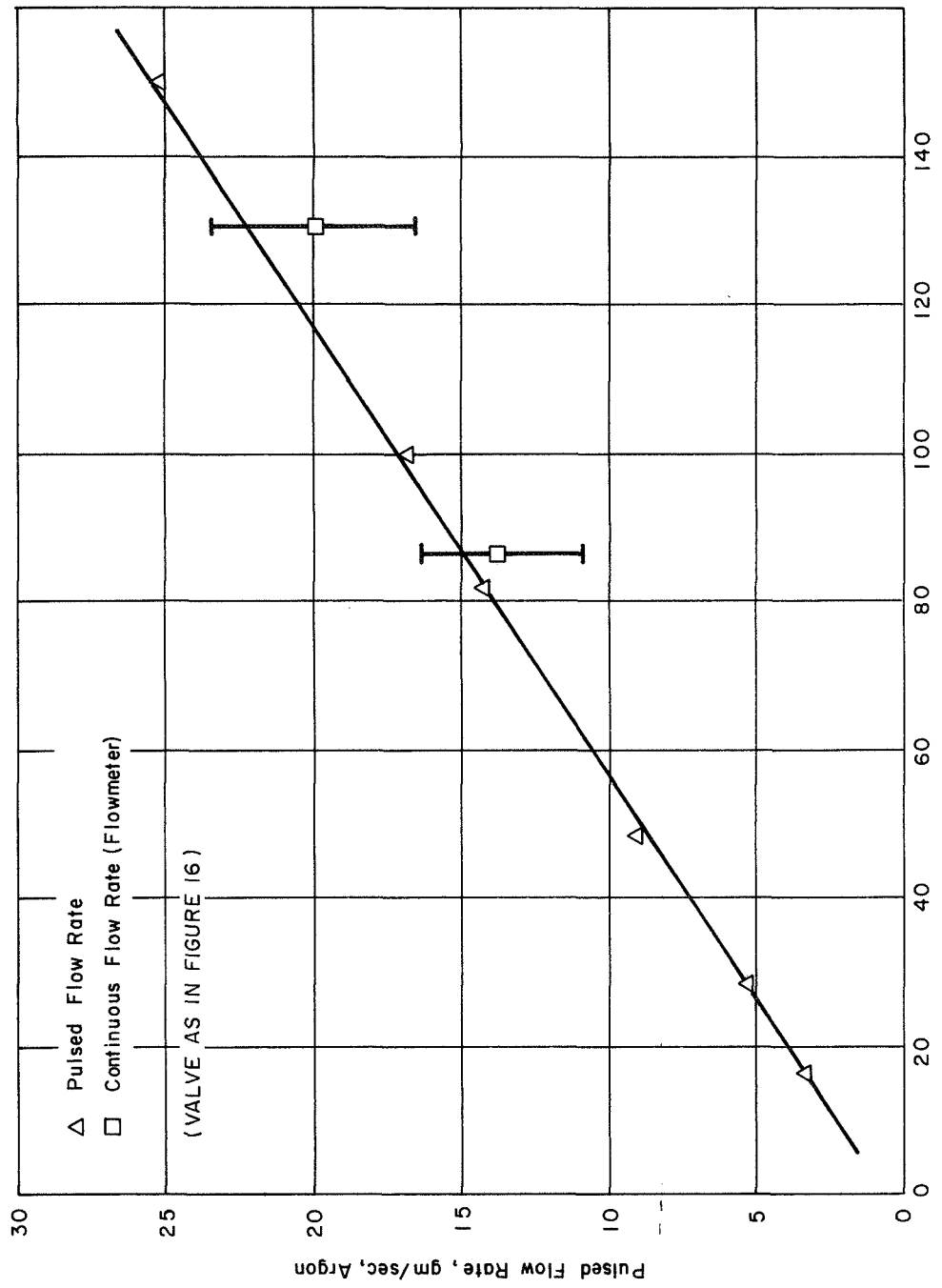

Figure 17 PULSED FLOW RATE VERSUS RESERVOIR PRESSURE

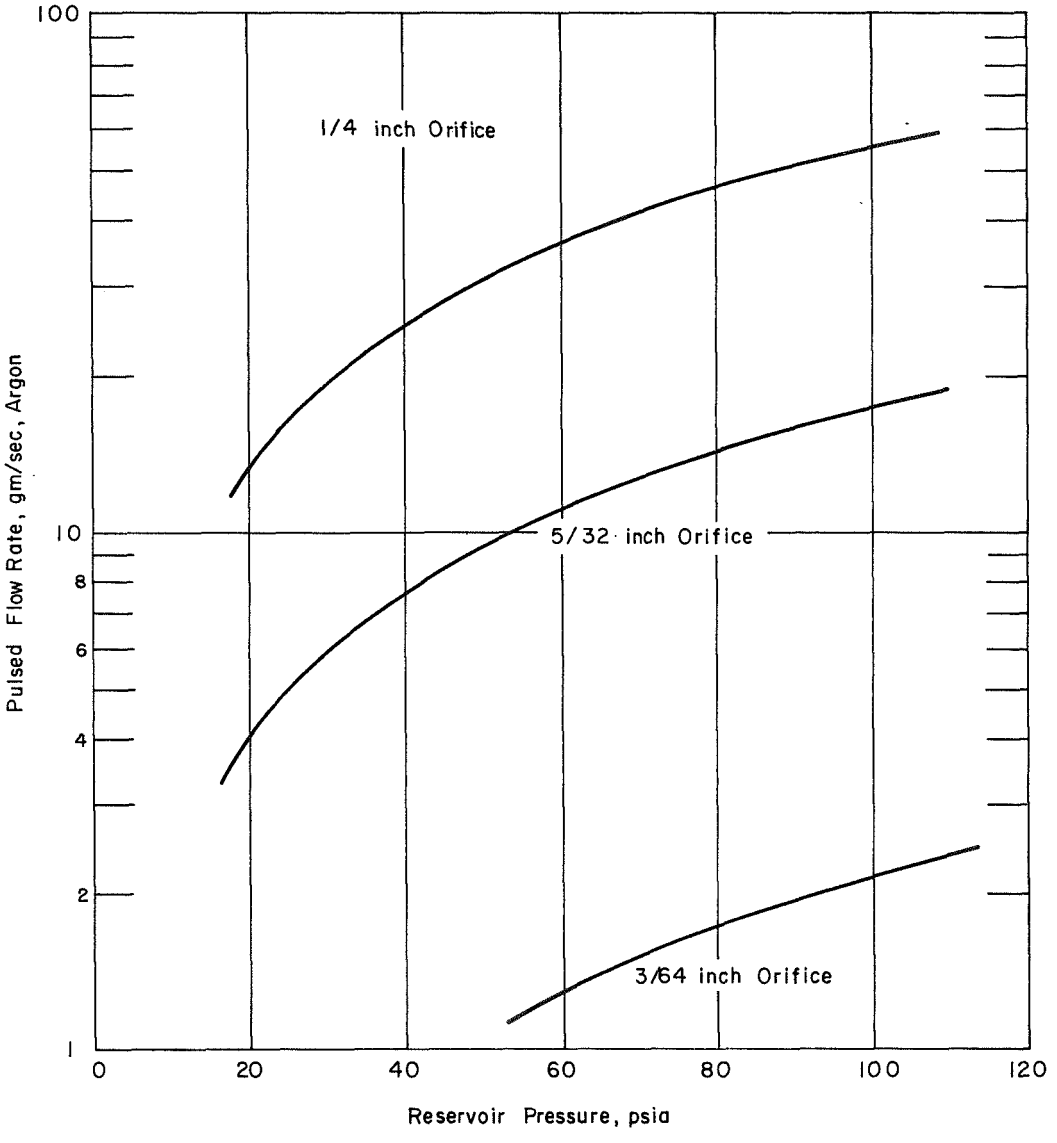

Figure 18 PULSED $\dot{m}$ VERSUS RESERVOIR PRESSURE FOR THREE DIFFERENT VALUES
(Middle Plot Refers to Data and Value of Figures 16 and 17)

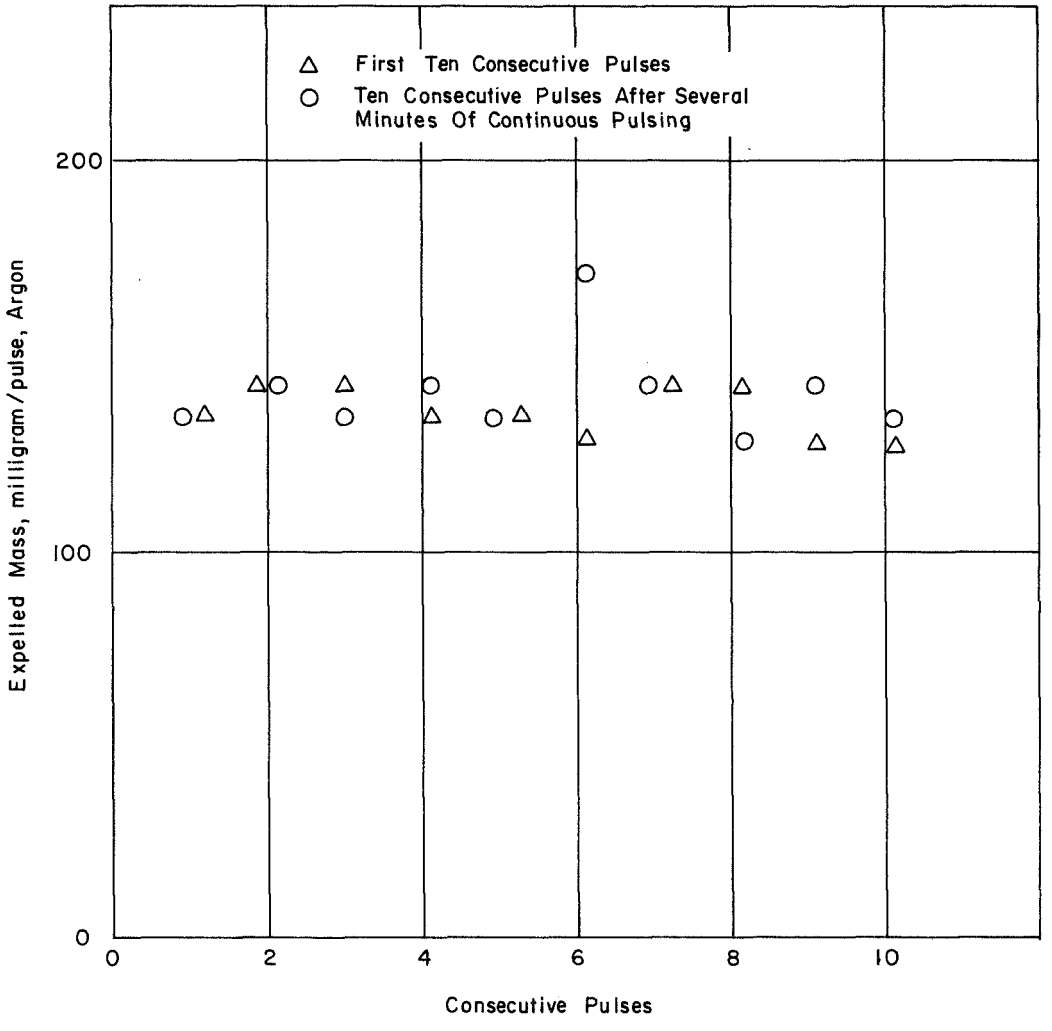

Figure 19 REPRODUCIBILITY TEST FOR THE VALVE OF FIGURE 16

4. Transient Probing

The $\dot{m}$ pulses are now investigated temporally and spatially with the help of the Varian, Millitorr Gauge. The gauge output is naturally related (by calibration) to the pressure magnitude at any given time and spatial station. In turn, pressure may be related to gas density and (for given flow conditions) to $\dot{m}$ magnitude.

Two very important parameters are obviously the onset delay of the $\dot{m}$ pulse at any given station and the rise time of the $\dot{m}$ magnitude, say from the 10 to the 90 percent level of the steady state magnitude. These quantities depend on several parameters of the overall system. Most important are:

(a) electrical inertia for valve activation,

(b) mechanical inertia of the valve,

(c) flow resistance between valve and accelerator,

(d) volume to be filled with gas before steady flow is established, and

(e) response time of the sensor.

Naturally, the detailed flow pattern must also be considered and examined, if probing is desired at flow stations well downstream of the accelerator exit.

In the work reported here, reasonable efforts were made to minimize the mentioned factors, without undertaking a major development program. In the reported experimental results, the illustrated onset delay and rise times result from the collective action of all mentioned factors.

Refer to Figure 20, which presents examples of onset delay and rise times. It is easily seen that, by increasing the pulse voltage which activates the valve, both the onset delay and the rise times are very substantially improved.

Before further discussion, it must be noted that such results are remarkably reproducible, as shown by the illustrations of Figure 21. Next, we consider the calibration of pulse amplitudes in terms of mass flow rate. In essence, the output of the Millitorr Gauge (in microamperes, or millivolts corresponding to a known load resistance) may be related to the static pressure with the help of the gauge calibration shown in Figure 14. For example, in the data of Figures 20 and 21, the steady state amplitude is about 5 microamps which, according to Figure 14, implies a pressure of 0.5 torr. Up to this pressure, a linear response may be expected (Figure 14). Because for one and the same geometry, and for identical pulse shapes, we expect the pressure at a given station to be proportional to $\dot{m}$, we may also expect the gauge output to be proportional to the $\dot{m}$. This has been verified, and will be discussed.

An example of $\dot{m}$ calibration is now discussed. Refer to Figure 22a which shows the complete pulse, as diagnosed at the accelerator exit. The experimental conditions as well as the onset and rise time of this pulse were illustrated in Figure 20c. The intended activation time of the valve is about 4 milliseconds, although the steady state of $\dot{m}$ lasts at least 10 milliseconds. However, this is of secondary importance compared with the fact that the onset delay time is about 1.5 milliseconds and the rise time about 0.5 millisecond, both of which are reproducible

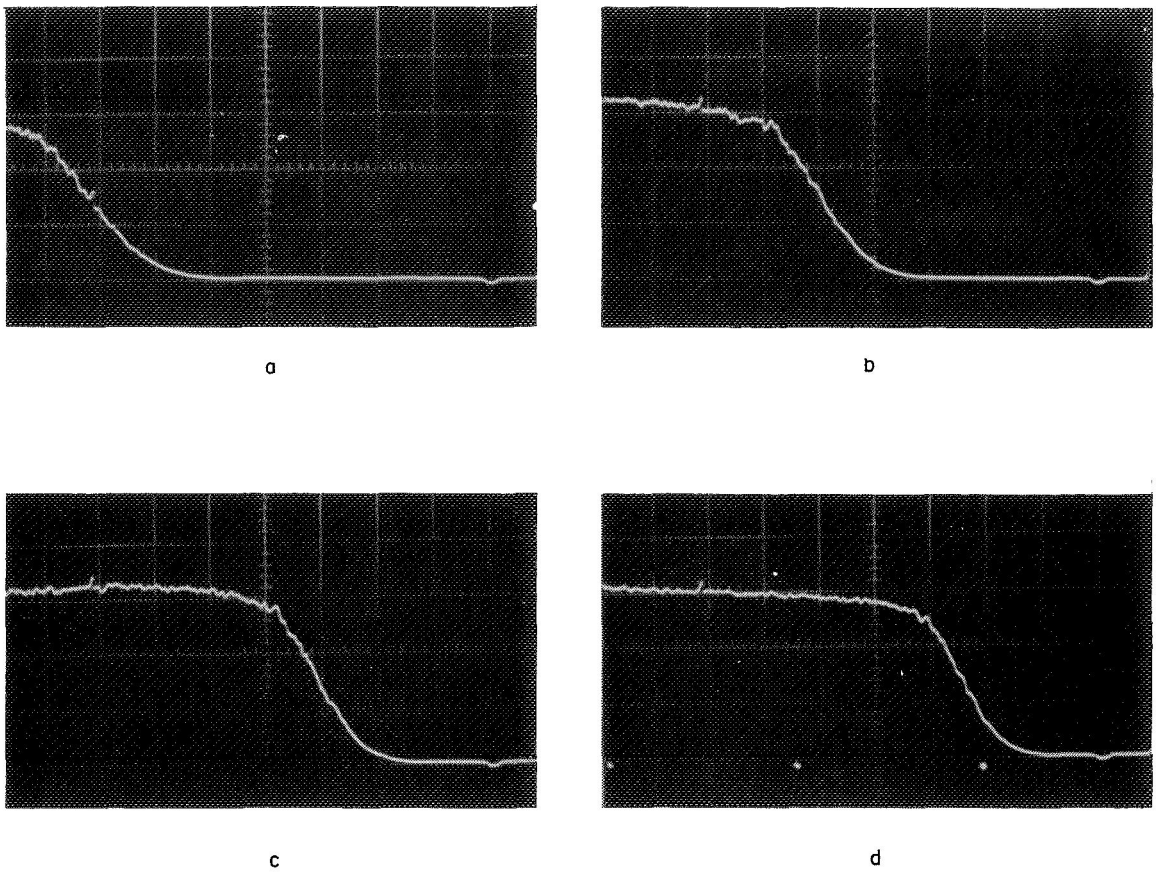

Figure 20 EXAMPLES OF ONSET DELAY AND RISE TIMES OF A 10 gm/sec PULSE AS DETERMINED BY THE TRANSIENT PRESSURE GAUGE AT THE EXIT PLANE OF THE ACCELERATOR, ON THE CENTERLINE
(MilliTorr Gauge Output, 1.7 MicroAmps/cm, versus Time, 500 Microseconds/cm. The Sweep is Initiated at the Extreme Right of Each Frame, by the Same Pulse Which Activates the Valve to Open. The Four Examples (a), (b), (c) and (d) Refer Correspondingly to 13, 20, 40 and 60 Volts, for the Electrical Pulse Activating the Valve.)

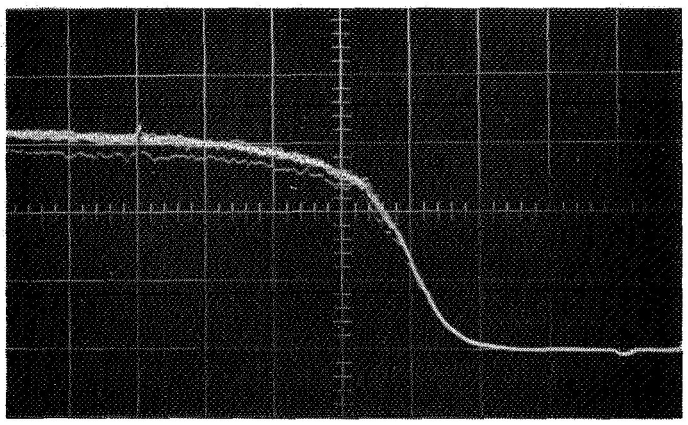

An overlay of 10 consecutive pulses of the example of Fig. 20c at a rate of 1 per second

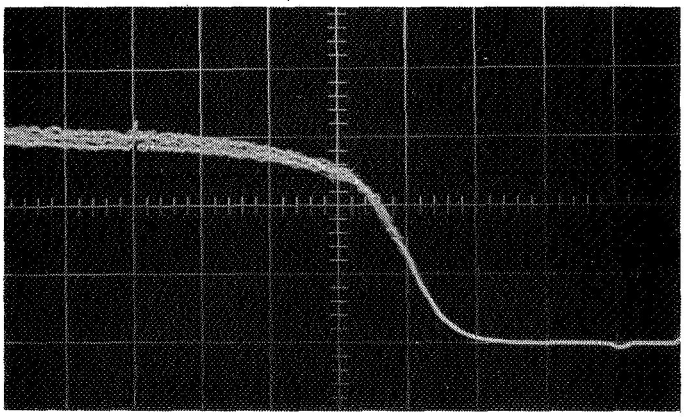

A similar overlay of 10 consecutive pulses, after several minutes of continuous pulsing at 1 pps

Figure 21 REPRODUCIBILITY TEST

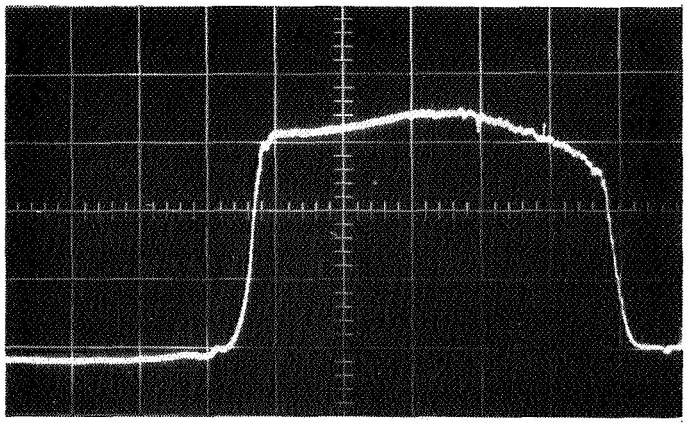

a.

Complete pulse for which the onset and rise are shown on the expanded sweep of Fig. 20c

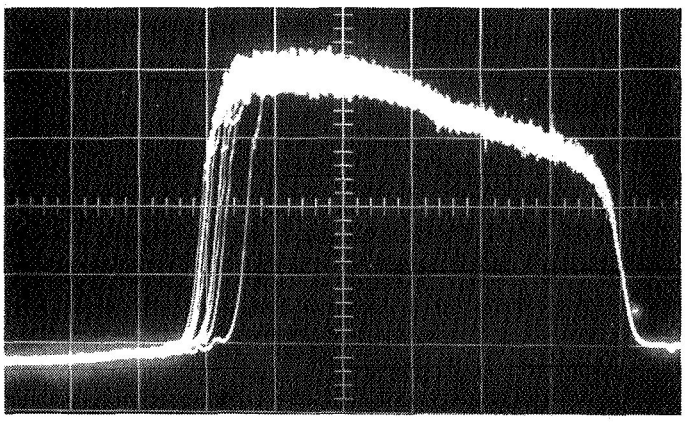

b.

An overlay of 10 consecutive pulses under approximately the same conditions, as in the upper frame

Figure 22 EXAMPLES OF $\dot{m}$ PULSES, WITH AN AMPLITUDE OF ABOUT 10 gm/sec, PROBED AT THE ACCELERATOR EXIT AND ON THE CENTERLINE
(Elapsed Time from Right to Left at 2 milliseconds/cm)

as discussed previously. The general shape of the pulse, as shown in Figure 22b is also reproducible.

The gauge output in Figure 22a is not saturated. This is experimentally confirmed and is so for $\dot{m}$ up to 10 gm/cm, at the accelerator exit (higher flow rates at further downstream stations). Consequently, the gauge output may be considered proportional to $\dot{m}$, and the integral of $\dot{m}dt$ under the pulse is proportional to the mass expelled by the valve, during this pulse. As discussed earlier in this report, the expelled mass per pulse is easily and independently measured, which provides the information necessary for calibration.

As expected, the pulses become sharper or blunter at stations inside or downstream of the accelerator exit, respectively. The effect is rather marginal for stations inside the chamber. However, downstream of the exit, the pulses become substantially blunter as may be seen by comparing the shapes of Figures 20b and 20d with those of Figures 23a and 23b, correspondingly. The only difference here is that the probed station has moved from the accelerator exit to about 2.5 inches (one exit diameter) downstream. Longer onset delays and longer rise times are evident.

Further examples of $\dot{m}$ pulses are presented in Figure 24, which correspond to a probing station 2.5 inches downstream of the exit. The valve is activated with 40 volts, 4 milliseconds electrical pulses. Because at this downstream station the gauge output saturates well above 20 gm/sec, a linearity test is possible over a fairly wide range of $\dot{m}$. To a fair approximation, we find both the $\dot{m}$ pulse amplitudes and the $\dot{m}dt$ integrals, for each pulse, proportional to the intended flow rates.

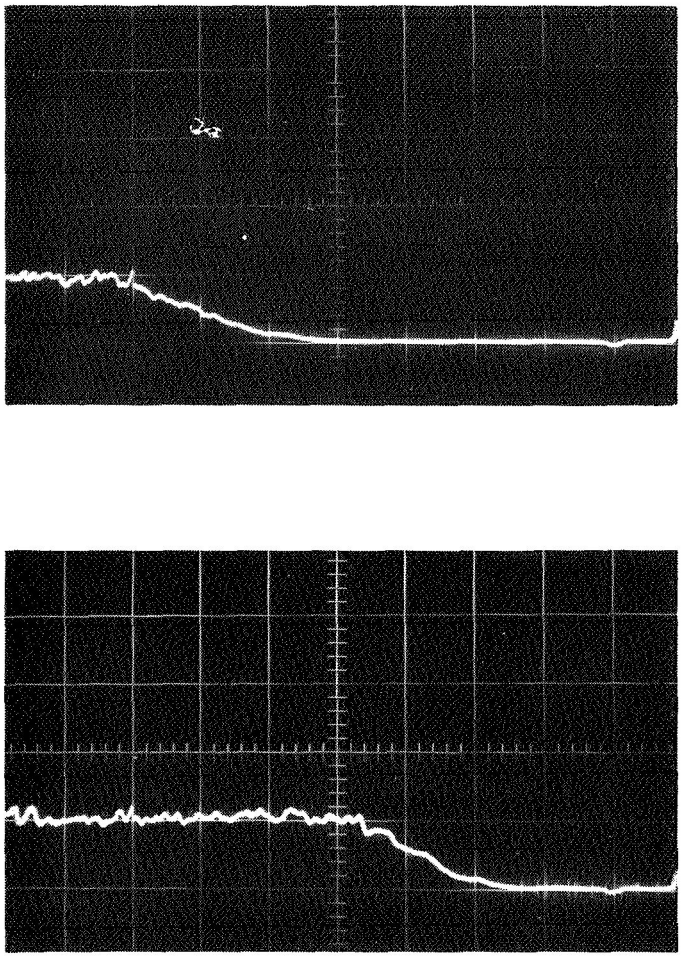

Figure 23 EXAMPLES OF ONSET DELAY AND RISE TIMES FOR A 10 gm/sec PULSE AS DETERMINED AT 2.5 inches DOWNSTREAM OF THE ACCELERATOR EXIT, ON THE CENTERLINE
(Cases a and b are Recorded under Conditions Identical to Those of Figure 20b and d, Including the Same Sweep Rates and Vertical Sensitivities)

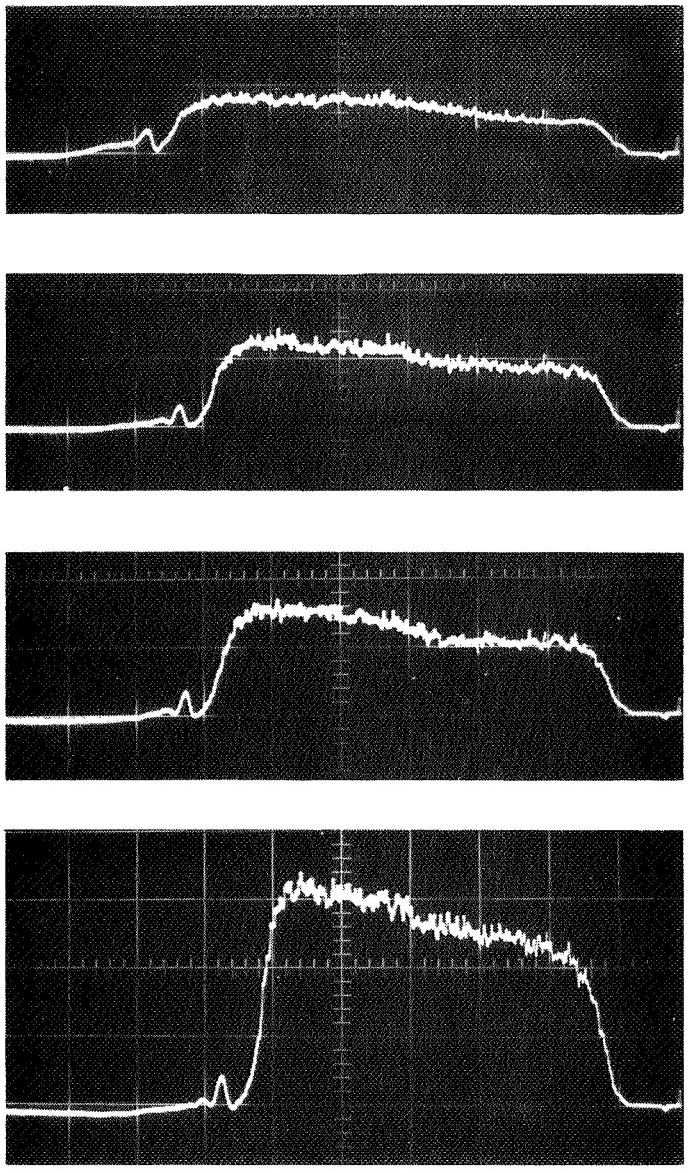

Figure 24 EXAMPLES OF $\dot{m}$ PULSES RECORDED AT 2.5 inches DOWNSTREAM OF THE ACCELERATOR EXIT, AT 2 milliseconds/cm
(The m Amplitude is Progressively Increased: 4, 8, 10, and 21 gm/sec. The Total Mass Contained in Each Pulse is about 50, 95, 120, and 250 Milligrams, Respectively.)

Finally, an idea of the gas density distribution, axially and radially, may be obtained from the data of Figures 25 and 26, where the Millitorr Gauge output has been converted into pressure. In Figure 25, Z = 0 corresponds to the accelerator exit. For relatively high flow rates, e.g., 10 gm/sec or higher, no pressure data inside the chamber are possible because of gauge saturation.

C. PULSED POWER

High power pulses were provided by discharging energy stored in a bank of electrolytic capacitors into the MPD accelerator. A total of 36 electrolytic capacitors (each about 3000 microfarads, rated at 350 volts) was used. This is a total of about 10^{-1} farads with an ultimate capability of storing 6000 joules. This capacitance, plus a total inductance of about 10 microhenries, were divided into four nearly equal sections, and a pulse forming network was obtained. This network has a characteristic impedance of $L/C^{\frac{1}{2}}$, or about 10 milliohms which is in the vicinity of the expected accelerator impedance. The expected pulse duration from this network is 2 $(LC)^{\frac{1}{2}}$, or about 2 milliseconds.

An appreciable distortion of the mentioned parameters is generally expected because of substantial ohmic impedance associated with electrolytic capacitors. In our case, the ohmic impedance (per each of the four sections of the pulse forming network) was found comparable to the MPD impedance. Evidence of this is found in the fact that approximately one half of the energy stored in the capacitors does not reach the MPD load.

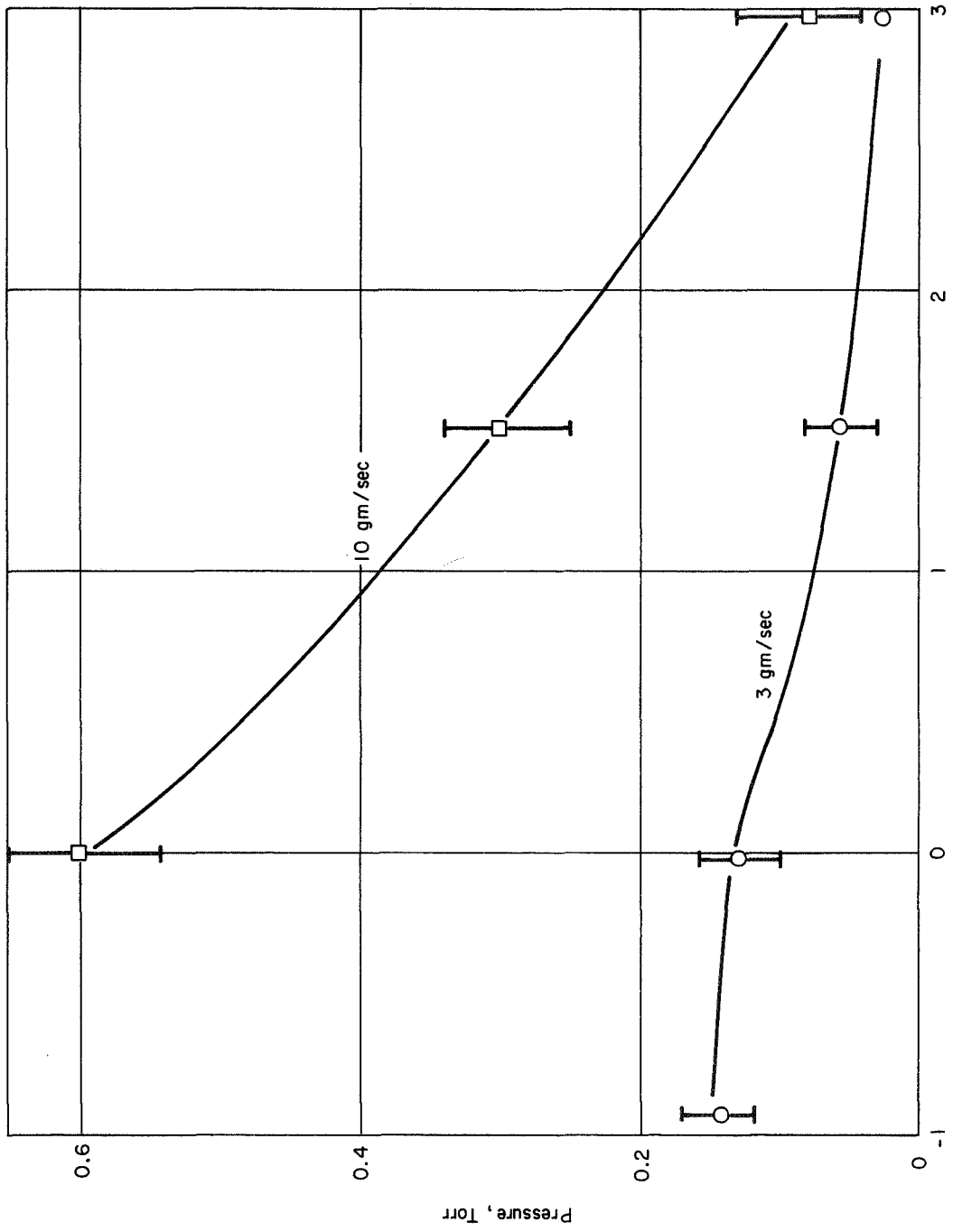

Figure 25 PRESSURE ON THE CENTERLINE VERSUS AXIAL DISTANCE AT TWO DIFFERENT PULSED FLOW RATES

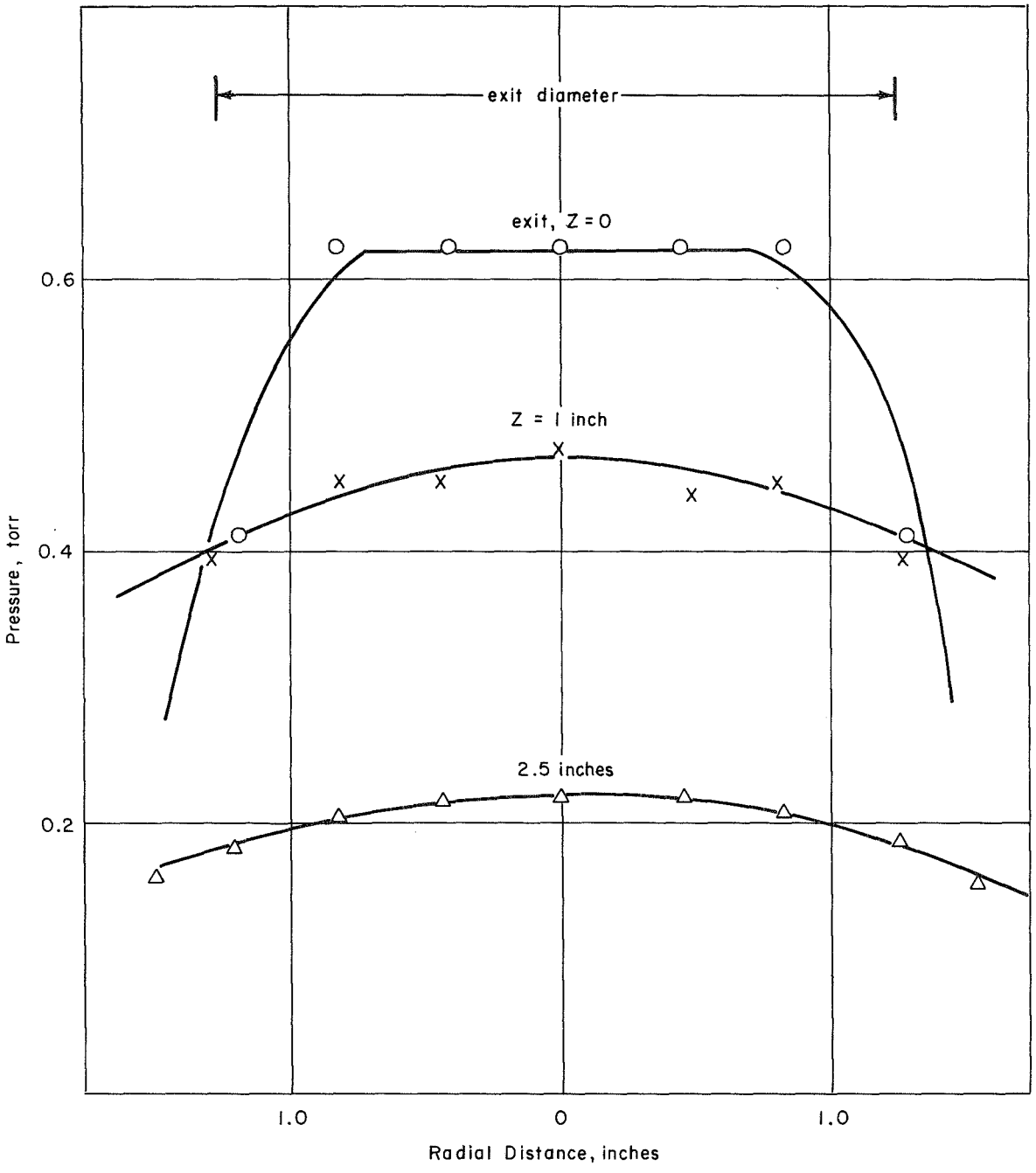

Figure 26 PRESSURE VERSUS RADIAL DISTANCE AT THREE DIFFERENT AXIAL STATIONS AND AT APPROXIMATELY 10 gm/sec

Electrical energy from an ordinary power supply was stored in the capacitor bank at voltages up to 300 volts. The MPD accelerator could very easily stand this voltage without breakdown even at the presence of an argon mass flow rate. Thus, the need of a switch was eliminated. In our present arrangement, MPD breakdown and power pulse delivery is initiated at will by a high voltage pulse, coupled to the MPD as shown in Figure 27. The coupling transformer is formed simply by a few turns around the last inductor of the MPD pulse forming network.

The trigger module in Figure 27 is fed by a pulse delayed by any desirable delay relative to the pulse which activates the valve to open. (See SCR_1, in Figure 13.) A delay of 3 to 4 milliseconds is found convenient, because this is usually the time between valve activation and the establishment of a steady flow rate.

A calibrated Rogowski coil and a voltage probe are used to record the current and voltage waveforms at the MPD. Two examples are illustrated in Figure 28. The voltage to current ratios in these data imply an MPD impendance in the vicinity of 4 milliohms which is substantially smaller than the 10 milliohms value used for general design. Superimposed on this mismatch is the fact that the capacitance, in each of the sections of the pulse forming network, has an internal impedance of the order of few milliohms. This, in essence, means that a substantial fraction of the stored energy is dissipated in the pulse forming network during each pulse. Evidence of this may be found in the fact that the pulse energy (time integrated products of current voltage) in the examples of Figure 28 accounts for approximately 2000 joules which is only half of the 4000 joules stored energy.

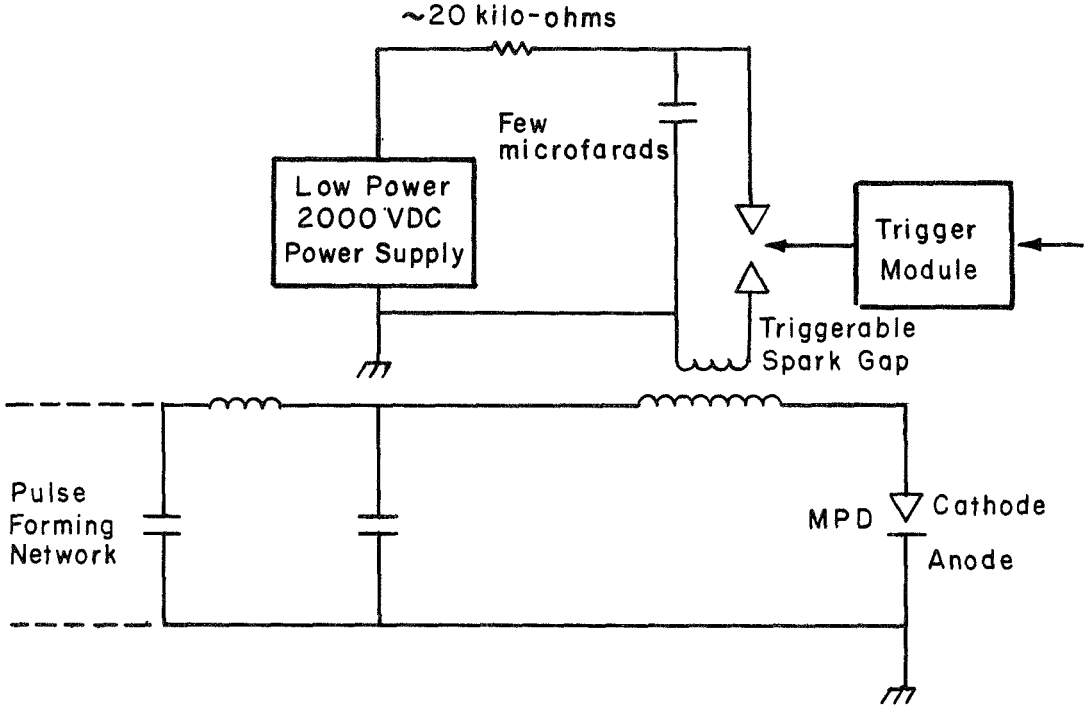

Figure 27 INDUCTIVE COUPLING OF A HIGHER VOLTAGE PULSE FOR MPD BREAKDOWN

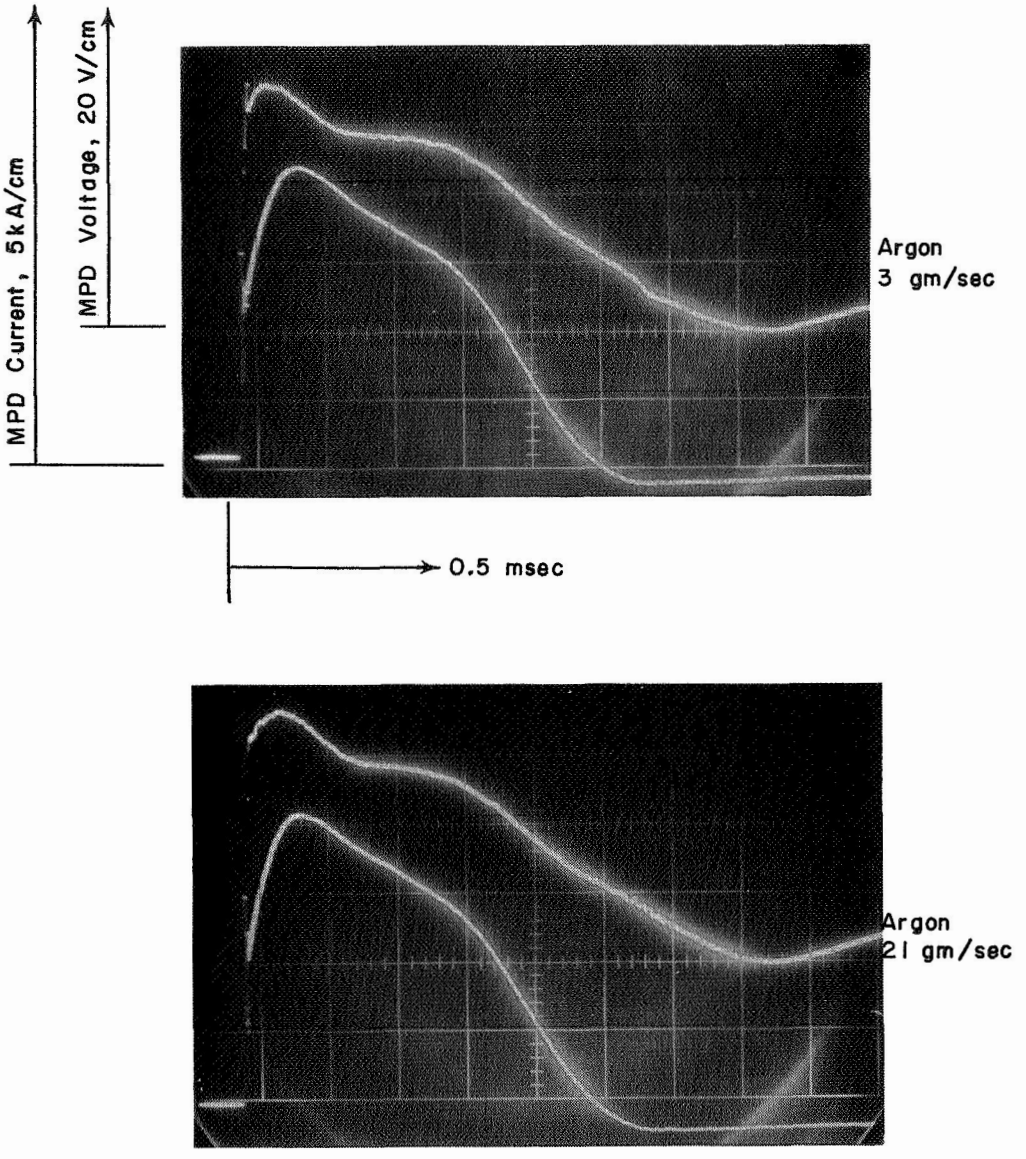

Figure 28 CURRENT AND VOLTAGE WAVEFORMS AT THE MPD STORED ENERGY: 4000 Joules

All these effects are clearly undesirable, however, the pulses of Figure 28 are considered acceptable for the purpose of initiating the diagnostics of the motional state of the propellant in high power quasi-steady MPD operation.

D. DIAGNOSTIC ARRANGEMENTS FOR DOPPLER SHIFT MEASUREMENTS

It is easily realized that the experimental arrangements for Doppler shift measurements, in the high power pulsed MPD, are not as simple and straightforward as in the steady state case. One serious difficulty arises from the fact that radiation is not continuously available. Thus, even in the case of a regularly and repetitively pulsed MPD, the photoelectric scanning of spectral lines is very cumbersome and a very large number of pulses may be required for a single shift determination. Thus, we must resort to photographic recording of spectra which, for the particular application under consideration here, is less convenient.

1. Need for Time Resolution

The current pulses delivered to the MPD are not ideally rectangular. Moreover, the intensity of line radiation is not necessarily in step with the amplitude of the MPD current pulse. Refer to Figure 29 which shows that substantial radiation may be emitted after the MPD current has decayed to values which are unimportant from the acceleration point of view. Thus, an appropriate shutter arrangement must be made to prevent the undesirable radiation from falsifying the Doppler shift measurements.

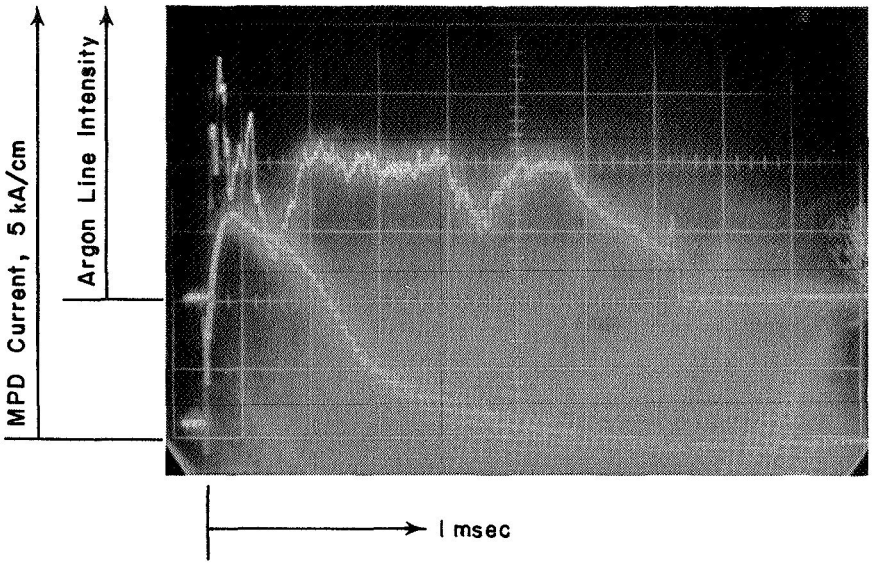

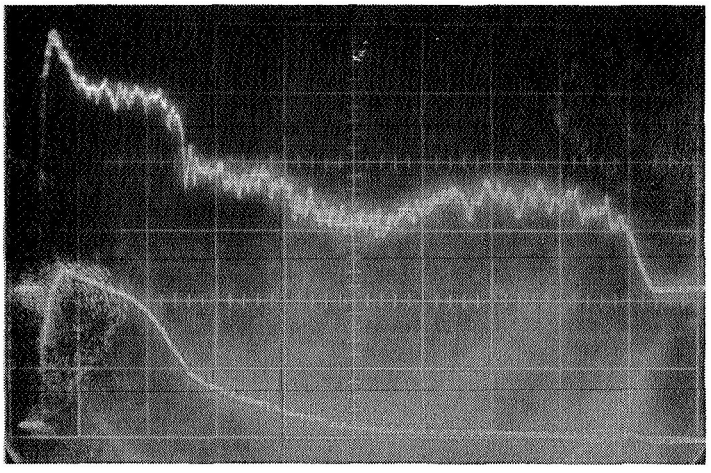

Figure 29 EXAMPLES OF SIMULTANEOUS RECORDINGS OF ARGON LINE INTENSITIES AND MPD CURRENT

2. Shutter

A shutter is desirable in front of the slit of the spectrograph, used for the Doppler shift measurements. This shutter should remain open for times between a few hundred microseconds and a few milliseconds, at any desirable stage, during the delivery of a power pulse to the MPD.

In the laboratory, shutter action is provided by a disc rotating in front of the spectrograph slit. The disc blocks the spectrograph at all times, except when a slot on the periphery of the disc passes by the spectrograph slit. If the shutter slot has a width w_s and is located at a radial distance r_s from the axis of rotation, then the shutter is effectively open during a time interval

$$t_o = w_s / 2n r_s f \tag{15}$$

where f is the rotation frequency of the disc. In actual practice, for the shutter we may use a slot width of 1 mm at a radius of about 17 cm with a disc rotating at 150 rpm. The resulting interval of open shutter is about 350 microseconds, which is quite adequate for the time resolution desired in our experiments. Both the slot width and the rotation frequency of the disc may be used for adjusting the exposure time.

3. Shutter Synchronization and Repetition Rate

It is understood that the shutter should open at any desirable stage, preferably immediately following the initiation of a power pulse to the MPD. Moreover, this should be done at any desirable rep rate. Presently, it is found more convenient to synchronize the MPD activation events to the shutter, rather than the other way around.

A signal for repetitive operation could, in principle, be provided by the same disc which operates the shutter. However, this would be inconvenient because the rep rate would have to be coupled with the rotation frequency which appears in Eq. (15). To maintain a rep rate independent of the shutter rotation frequency, a smaller secondary disc is employed. This secondary disc is coupled to the same, (150 rpm), motor as the shutter disc, however its coupling is geared down by a factor of three, so it rotates at 50 rpm or about once every 1.2 seconds. In practice, a small hole on the disc allows an ordinary light beam to activate an auxiliary photomultiplier, at the specified rep rate. Moreover, it is easily arranged so that the shutter slot is found at any desirable angular distance from the spectrograph slit, when the auxiliary photomultiplier is activated. This angular distance, divided by the angular velocity of the shutter disc, gives the time delay between photomultiplier activation and the beginning of spectrograph slit exposure. The duration of the exposure is determined by Eq. (15).

In actual practice, the repetitively available signal from the auxiliary photomultiplier is used to trigger the complete MPD sequence as shown in Figure 30. Variable Delay Generator 1 is used to delay the initiation of the MPD cycle by any length of time necessary for the coincidence of the spectral exposure with any desirable phase of the MPD cycle. The output of Delay Generator 1 is split into three signals. One of these is used directly to activate the initiation of the mass flow pulse. The second signal is fed into Delay Generator 2 where it is delayed, usually by 4 milliseconds, which is sufficiently long for the $\dot{m}$ pulse to arrive at the interelectrode region and to reach steady state.

The delayed pulse, under consideration here, triggers the trigger module of Figure 27 and initiates the delivery of the power pulse. Finally, a third signal from Delay Generator 1 is fed into Delay Generator 3. Here, with a usual delay of 7 milliseconds, a pulse is provided for closing the valve. It is understood that this delay should be equal, at least, to the sum of Delay 2 plus the power pulse duration.

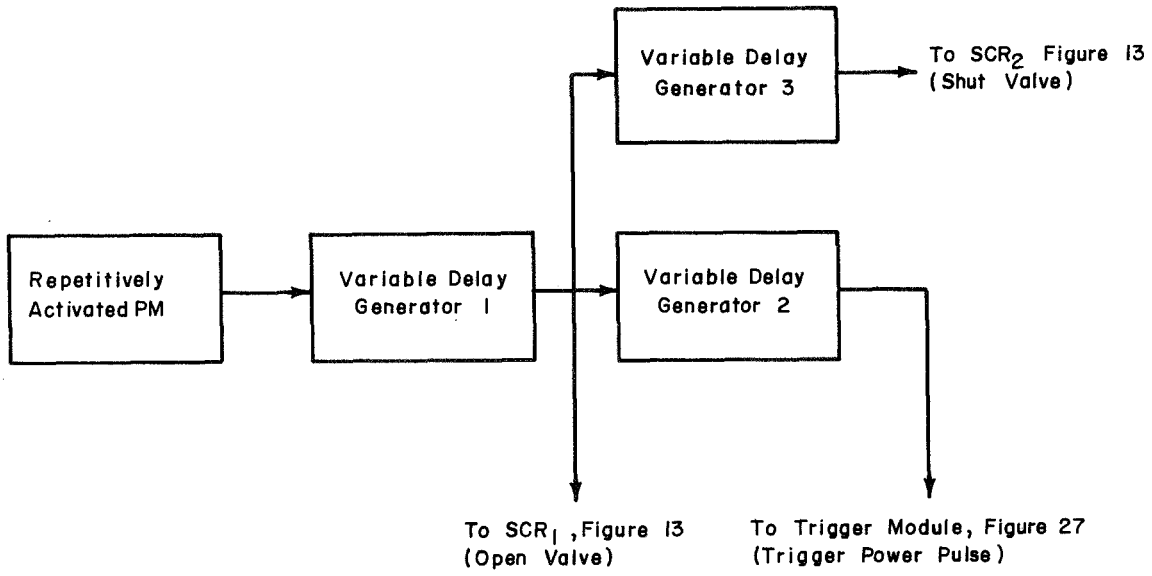

Figure 30 SCHEMATIC OF TRIGGER ARRANGEMENTS FOR A COMPLETE PULSED MPD CYCLE

An application of the shutter in operation is illustrated in Figure 31. The following additional information is relevant. The parameters, appearing in Eq. (15), have the values: w_s = 5 mm, r_s = 17 cm, and f = 150 rpm. It follows that the exposure duration is approximately equal to 2 milliseconds. This is generally desirable because the MPD power pulse has about the same duration. (See Figure 29.)

The same power pulse is used in the examples of Figure 31. In Figure 31a an argon line intensity is recorded, without shutter action, in a fashion similar to that of Figure 29. In the examples of Figures 31b, c and d, the shutter is used with an approximate exposure of 2 milliseconds. This exposure is synchronized to begin: (a) immediately following the initiation of the 2 millisecond power pulse, (b) 3 milliseconds later and (c) 4 milliseconds later.

Thus, a 2 millisecond window, exposing the spectrograph slit to MPD radiation, may be arranged to coincide with any desirable phase of the MPD pulse. Much shorter exposures may be arranged by making the shutter slot narrower and/or by increasing the rotational rate of the shutter disc.

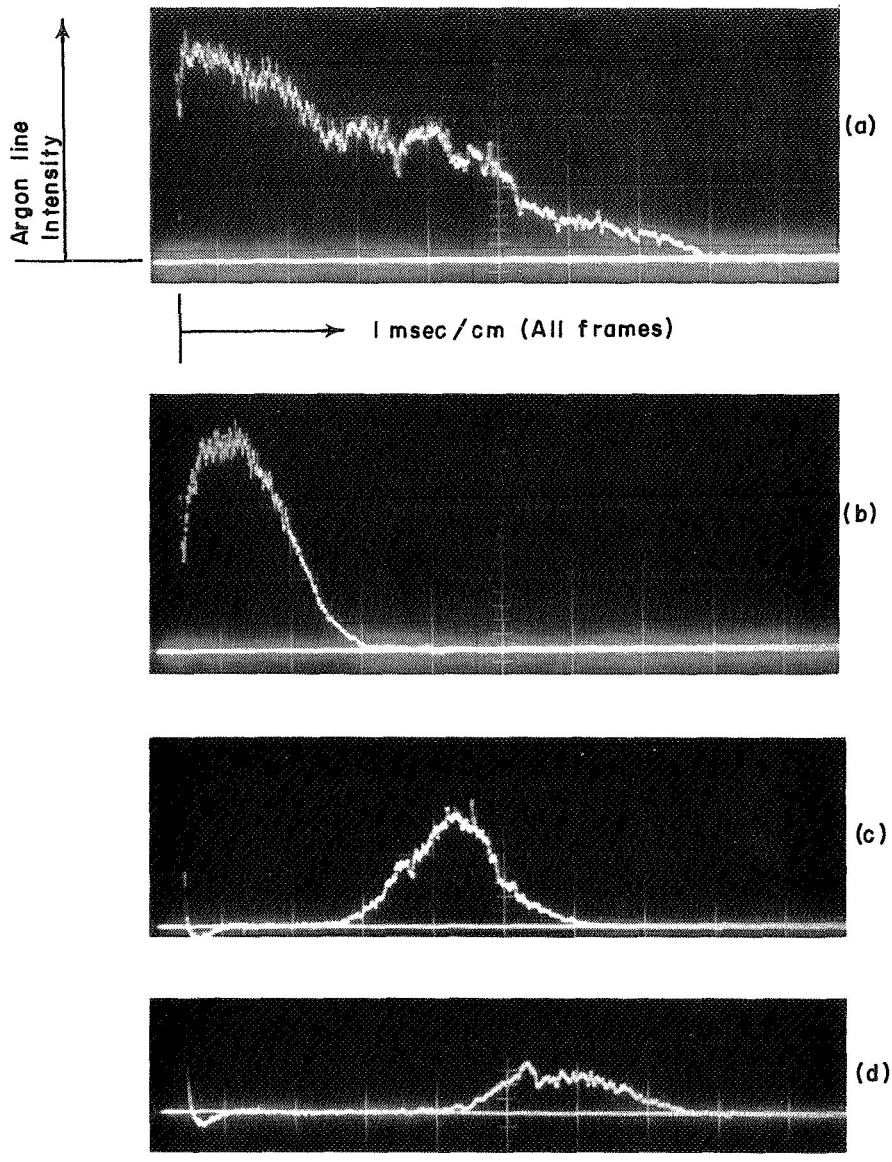

Figure 31 ARGON LINE INTENSITY
(a: Corresponding to a 2 millisecond Power Pulse (See Figure 29.) b, c. and d: Illustration of Shutter Operation with a 2 millisecond Window, Immediately Following Power Pulse Initiation, 3 milliseconds and 4 milliseconds Later.)

REFERENCES

1. Malliaris, A., and Libby, D. R.: Velocities of Neutral and Ionic Species in an MPD Flow. AIAA paper, 69-109, 1969.
2. Kogelschatz, V.: Doppler Shift Measurements of Axial and Rotational Velocities in an MPD Arc. AIAA paper, 69-110, 1969.
3. Kruelle, G.: Characteristics and Local Analysis of MPD Thrustor Operation. AIAA paper 67-672, 1967.
4. Bohn, W.: Institute of Plasmadynamics. Stuttgart, West Germany, Private Communication.
5. Sovie, R., and Connolly, D.: A Study of the Axial Velocities in an Ammonia MPD Thrustor, AIAA Journal, Vol. 7, No. 4, April 1969, pp. 723-725.
6. Connolly, D., and Sovie, R.: The Effect of Background Pressure and Magnetic Field Shape on MPD Thrustor Performance. AIAA paper, 69-243, 1969.
7. Malliaris, A.: Oscillations in an MPD Accelerator. AIAA Journal, Vol. 6, No. 8, August 1968, pp. 1575-1577.
8. Malliaris, A.: Plasma Acceleration in an Electrical Discharge by the Self-Induced Magnetic Field. Journal of Applied Physics, Vol. 38, No. 9, August 1967, pp. 3611-3619.
9. Malliaris, A.: Interaction of an Electrical Discharge with its Self-Induced Magnetic Field in the Presence of Gas Flow. Aerospace Research Laboratories, Technical Report, ARL 67-0007, January 1967.
10. Powers, W.: Measurements of the Current Density Distribution in the Exhaust of an MPD Arcjet. AIAA Journal, Vol. 5, No. 3, March 1967, pp. 545-550.
11. Yos, J.: Theoretical and Experimental Studies of High Temperature Gas Transport Properties. Avco Technical Report, RAD-TR-65-7, May 1965.

12. Malliaris, A., and Libby, D. R.: An Investigation of MPD Accelerators. Aerospace Research Laboratories Report, ARL 70-0011, January 1970.

13. Clark, K. E., and Jahn, R. G.: Quasi-Steady Plasma Acceleration. AIAA paper, 69-267, 1969.

NASA CR-111785

DISTRIBUTION LIST
NAS1-9298

	No. Copies
NASA Langley Research Center Hampton, Virginia 23365	
Attention: Research Program Records Unit, Mail Stop 122	1
Raymond L. Zavasky, Mail Stop 117	1
Joseph Burlock, Mail Stop 160	25
NASA Ames Research Center Moffett Field, California 94035	
Attention: Library, Mail Stop 202-3	1
NASA Flight Research Center P. O. Box 273 Edwards, California 93523	
Attention: Library	1
Jet Propulsion Laboratory 4800 Oak Grove Drive Pasadena, California 91103	
Attention: Library, Mail 111-113	1
NASA Manned Spacecraft Center 2101 Webster Seabrook Road Houston, Texas 77058	
Attention: Library, Code BM6	1
NASA Marshall Space Flight Center Huntsville, Alabama 35812	
Attention: Library	1
NASA Wallops Station Wallops Island, Virginia 23337	
Attention: Library	1
NASA Lewis Research Center 21000 Brookpark Road Cleveland, Ohio 44135	
Attention: Library, Mail Stop 60-3	1
NASA Goddard Space Flight Center Greenbelt, Maryland 20771	
Attention: Library	1
John F. Kennedy Space Center Kennedy Space Center, Florida 32899	
Attention: Library, Code IS-CAS-42B	1

NASA CR-111785

DISTRIBUTION LIST (Concl'd)
NAS1-9298

	No. Copies
National Aeronautics & Space Administration Washington, D. C. 20546	
Attention: Library, Code USS-10	1
NASA Code RN	1
NASA Scientific and Technical Information Facility P. O. Box 33 College Park, Maryland 20740	12 plus reproducible
Research Library--Wilmington	3
Research Library--Lowell	1
Internal Distribution	20